Small Molecule and Pooled CRISPR Screens Investigating IL17 Signaling Identify BRD2 as a Novel Contributor to Keratinocyte Inflammatory Responses

Peter F. Slivka,*[†,∇] Chen-Lin Hsieh,[‡,∇] Alex Lipovsky,[†] Steven D. Pratt,[§] John Locklear,[§,‖] Marian T. Namovic,[§] Heath A. McDonald,[⊥] Joseph Wetter,[⊥] Rebecca Edelmayer,[⊥] Min Hu,[‡] Erin Murphy,[‡] Marc Domanus,[‡] Charles Lu,[‡] Ryan Duggan,[#] Jacob King,[†] Victoria E. Scott,[⊥] Diana Donnelly-Roberts,[§] Anthony Slavin,[@] Sujatha Gopalakrishnan,[§] Namjin Chung,[‡] and Eric R. Goedken[†]

[†]Discovery Dermatology & Fibrosis, AbbVie Bioresearch Center, Worcester, Massachusetts 01605, United States
[‡]Genomics Research Center, AbbVie Inc., North Chicago, Illinois 60064, United States
[§]Target Enabling Science & Technology, AbbVie Inc., North Chicago, Illinois 60064, United States
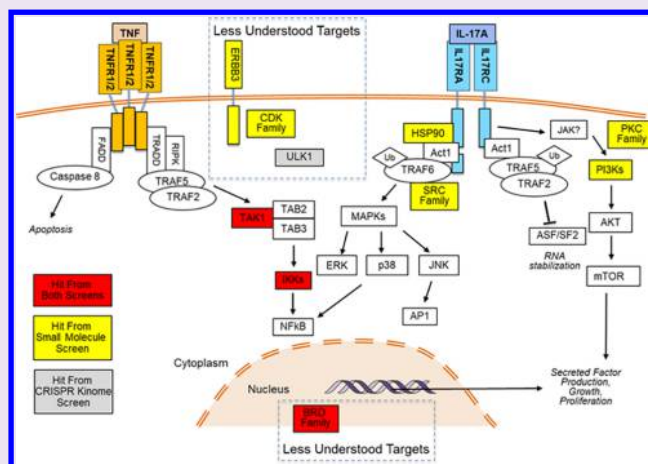[‖]PerkinElmer Life Sciences, Waltham, Massachusetts 02451, United States
[⊥]Discovery Dermatology & Fibrosis, AbbVie Inc., North Chicago, Illinois 60064, United States
[#]Immuno-Oncology Discovery, AbbVie Inc., North Chicago, Illinois 60064, United States
[@]Immunology Pharmacology, AbbVie Bioresearch Center, Worcester, Massachusetts 01605, United States

S *Supporting Information*

ABSTRACT: Interleukin-17A (IL17A) plays a critical role in the development of numerous autoimmune diseases, including psoriasis. The clinical success of IL17A neutralizing biologics in psoriasis has underlined its importance as a drug discovery target. While many studies have focused on the differentiation and trafficking of IL17A producing T-helper 17 cells, less is known about IL17A-initiated signaling events in stromal and parenchymal cells leading to psoriatic phenotypes. We sought to discover signaling nodes downstream of IL17A contributing to disease pathogenesis. Using IL17A and tumor necrosis factor α (TNF) to stimulate primary human epidermal keratinocytes, we employed two different phenotypic screening approaches. First, a library of ~22000 annotated compounds was screened for reduced secretion of the pro-inflammatory chemokine IL8. Second, a library of 729 kinases was screened in a pooled format by utilizing CRISPR-Cas9 and monitoring IL8 intracellular staining. The highest-ranking novel hits identified in both screens were the bromodomain and extra-terminal domain (BET) family proteins and bromodomain-containing protein 2 (BRD2), respectively. Comparison of BRD2, BRD3, and BRD4 silencing with siRNA and CRISPR confirmed that BRD2 was responsible for mediating IL8 production. Pan-BRD inhibitors and BRD2 knockout also reduced IL17A/TNF-mediated CXC motif chemokines 1/2/6 (CXCL1/2/6) and granulocyte colony stimulating factor (G-CSF) production. In RNA-Seq analysis, 438 IL17A/TNF dependent genes were reduced in BRD2-deficient primary keratinocytes. KEGG pathway analysis of these genes showed enrichment in TNF signaling and rheumatoid arthritis relevant genes. Moreover, a number of genes important for keratinocyte homeostasis and cornification were dysregulated in BRD2-deficient keratinocytes. In IL17A/TNF/IL22 stimulated three-dimensional organotypic raft cultures, pan-BRD inhibition reduced inflammatory factor production but elicited aberrant cornification, consistent with RNA-Seq analysis. These studies highlight a novel role for BRDs and BRD2 in particular in IL17A-mediated inflammatory signaling.

The IL17 family consists of six isoforms (IL17A−F). In healthy individuals, these proteins carry out a number of important immune surveillance functions, including clearance of infections and antitumor activity. Chronic overexpression of

these family members contributes to a number of autoimmune diseases.[1,2] IL17A in particular has been implicated in the development of psoriasis and psoriatic arthritis. Therapeutic antibodies neutralizing IL17A are highly efficacious in the clinic, reducing or eliminating disease symptoms in many psoriatic patients.[3,4] Despite the efficacy of these anti-IL17A biologics, only patients with severe disease (∼10% of all patients) typically receive these drugs due to the potential difficulties associated with injectable therapies.[5] As such, there is a distinct need to identify new drug targets that neutralize IL17A and its downstream effects.

In psoriasis, overexpression of IL17A activates IL17 receptors IL17RA and IL17RC on keratinocytes and fibroblasts.[6] Formation of this complex recruits the adaptor and ubiquitin ligase ACT1. ACT1 subsequently recruits and activates tumor necrosis factor α (TNF) receptor-associated factor (TRAF) molecules such as TRAF5 and TRAF6 (among others). With this initial complex as a starting point, a wide array of signaling pathways are activated in parallel, including nuclear factor κB essential modulator (NEMO)-dependent NFκB signaling, mitogen-activated protein kinase (MAPK)-driven activator protein 1 (AP1) signaling, phosphoinositide 3-kinase (PI3K) signaling, and CCAAT enhancer binding protein (C/EBP) signaling. Additionally, IL17A signaling can stabilize mRNA transcripts by sequestering splicing factor 2 (SF2) and preventing SF2-mediated mRNA decay. This mRNA-stabilizing effect allows IL17A to amplify inflammatory gene signatures mediated by other pro-inflammatory cytokines such as TNF and IL1β.[7] In addition to driving cytokine and chemokine inflammation, IL17A also contributes to cell growth and phenotypic changes. As such, IL17A is a key proliferative signal in psoriasis, driving the production of growth factors from keratinocytes and fibroblasts[8] while also reducing the level of cornification (the non-inflammatory apoptotic process of keratinocyte maturation) in the epidermis.[9] This combination of hyperproliferation and reduced differentiation of keratinocytes, together with the more widely studied IL17A effects such release of neutrophil chemoattractants, helps drive the psoriatic phenotype.[10]

Despite this understanding of some aspects of IL17A signaling, few novel approaches have emerged to complement the existing IL17-directed biologics and most current areas of interest in this space focus on limiting the production of IL17A from T-helper 17 (TH17) cells[11,12] or directly neutralizing IL17A.[13] For example, retinoic acid-related orphan receptor-γt (RORγT) is a key transcription factor involved in TH17 differentiation whose inhibition effectively prevents IL17A production. Multiple clinical trials have been initiated targeting RORγT with small molecules. Similarly, small molecule or peptide inhibitors of the IL17A cytokine itself with reasonable potency and in vitro efficacy have been identified.[13]

Notably, no tractable drug targets that inhibit downstream signaling pathways activated by IL17A have advanced. Moreover, there is no clear indication that neutralizing only one of the known pathways (or a subset) downstream from IL17A will lead to clinical efficacy. Only knockout of targets proximal to IL17A such as IL17RA or ACT1 appears to fully recapitulate the psoriasis-resistant phenotype, presumably through direct neutralization of IL17A signaling.[14,15] While there are reports showing that inhibition of kinases downstream from IL17A such as protein kinase C (PKC)[16] and PI3K family members[17] drives some efficacy in animal models, no downstream target has established itself as the frontrunner

for the next wave of IL17A-focused therapies. Moreover, many of the pathways utilized by IL17A are canonical pathways that are difficult to target due to toxicity issues and/or unexpected adverse events such as the dermatitis side effect associated with MEK1/2 inhibition.[18]

Given the lack of robust, tractable targets for drug discovery downstream of IL17A, we sought to identify novel, druggable nodes and pathways downstream from IL17A in an unbiased fashion. To accomplish this goal, we conducted two parallel phenotypic screens. IL17A and TNF were used to stimulate IL8 production in primary keratinocytes, and this assay was applied in two interrelated screens. An annotated small molecule library of ∼22000 compounds was screened to identify targets that reduce IL8 secretion (and thereby IL17A signaling), and a pooled CRISPR library knocking out 729 kinases was screened to identify targets whose repression will reduce IL8 intracellular expression. The combination of these two complementary methods provided an opportunity to compare the insights from both screens and facilitated prioritization of cross-validated targets.

The highest-ranking targets common to both the small molecule and kinome CRISPR library screens were BET family proteins and BRD2, respectively. BET family proteins, of which BRD2 is one, contain two N-terminal bromodomain structures that recognize acetylation patterns on chromatin. C-Terminal residues on BET proteins subsequently recruit transcription factors to mediate gene expression, including IL17A production in TH17 cells.[12,19] Multiple inhibitors targeting the dual-bromodomain structure shared by all BET family members (BRD2−4 and BRDT) have been described,[20,21] and administration of these compounds has been shown to reduce IL17A production both in vitro and in vivo using various TH17-dependent animal models.[12,22] BET family members also possess Ser/Thr kinase activity and phosphorylate multiple nuclear proteins, including transcription factors.[23] We found that inhibition of BET proteins with pharmacologic inhibitors also blocks downstream cytokine signaling, reducing IL17A/TNF-mediated IL8, CXCL1/2/6, and G-CSF production in primary keratinocytes. Knockdown of BRD2 but not BRD3 or BRD4 with siRNA and CRISPR also significantly decreased secreted factor production in these cells. Furthermore, we show that addition of pan-BRD inhibitors to IL17A/TNF/IL22-treated three-dimensional (3D) organotypic raft cultures significantly suppressed inflammatory factors but also altered keratinocyte cornification. These changes were distinct from the profile observed by inhibition of IκB kinase α and β (IKKαβ), which more robustly blocked IL17A signaling in both two-dimensional (2D) and 3D cell experiments. These data indicate BRD2 has a unique role in IL17A signaling and may represent a novel opportunity for drug discovery in this key pathway.

■ RESULTS AND DISCUSSION

In this work, we present the output of two related phenotypic screens designed to interrogate key nodes of action downstream of IL17A/TNF signaling in primary keratinocytes. Integrating primary cells into cell-based research programs has the potential to deliver more biologically relevant and meaningful data as cell lines do not always reliably maintain their fundamental cellular functions. However, relying on primary cells may also lead to donor-specific responses rather than broadly applicable results. To reduce the likelihood of donor-specific effects, we profiled IL17A-, TNF-, and IL17A/
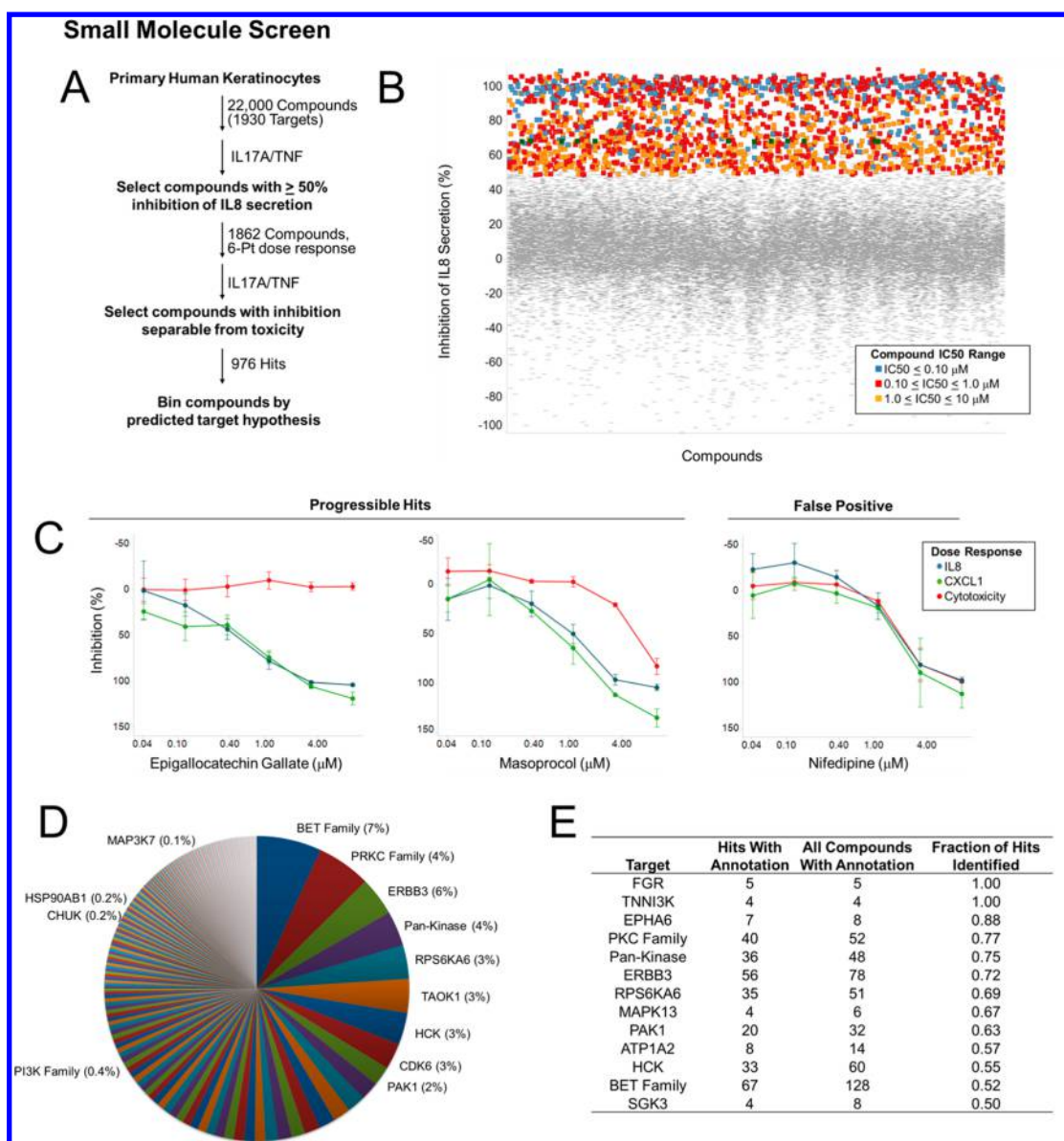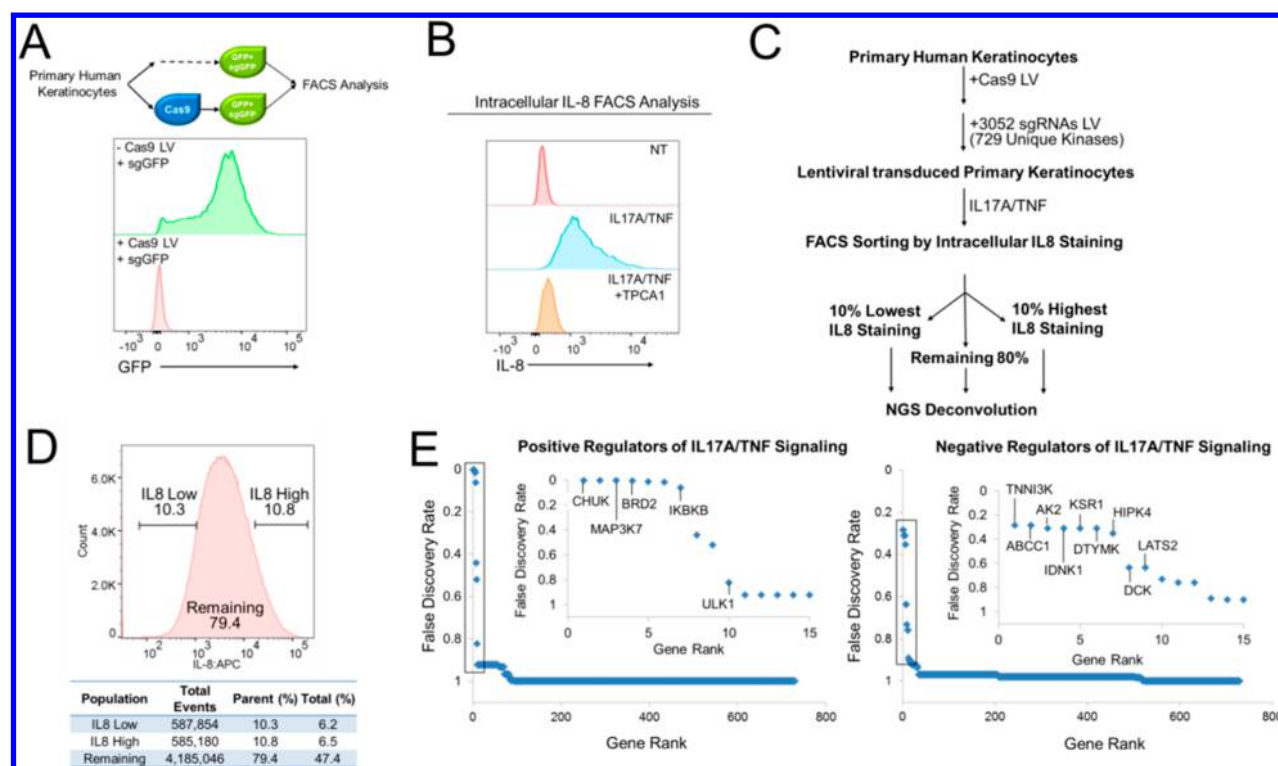
Figure 1. Overview of the screening strategy and hits from the annotated small molecule library. (A) A library of ~22000 compounds was screened in primary keratinocytes to identify compounds that inhibit IL17A/TNF-mediated IL8 secretion. (B) Dot plot from single-point (2.5 μM) screening of the library. Compounds with 50% inhibition of IL8 secretion were tested in six-point dose−response curves and are highlighted on the basis of their potency. (C) Sample−dose response curves depicting two progressible hits with noteworthy separation between IL8 and CXCL1 inhibition compared to cytotoxicity and one false positive with no chemokine inhibition separable from toxicity. Progressible hits were included for target analysis. (D) Using compound annotations, the number of positive hits for a given target was binned and expressed as a percentage of the total hits. (E) Target hypotheses were also ranked by comparing the number of hits for a given target vs the number of compounds in the library matching the target annotation.

TNF-mediated IL8 responsiveness in six independent keratinocyte donors (Supplementary Table 1). Notably, the IL17A and TNF responses across donors were very consistent. Screening metrics such as the Z′ factor and the IC$_{50}$ of a control compound TPCA1 (IKK$\alpha\beta$ inhibitor) were also consistent from donor to donor, further alleviating these concerns.

Two Orthogonal Screens of IL17A Action in Human Keratinocytes. To identify novel drug targets in the IL17A signaling cascade, two separate phenotypic screens were conducted using IL17A and TNF to drive IL8 production from primary human adult epidermal keratinocytes. First, ~22000 annotated small molecule compounds were screened at a single concentration of 2.5 μM, and 1862 compounds were

identified with 50% inhibition of IL8 secretion (Figure 1A,B). Compounds were subsequently examined in a six-point dose response to determine which compounds suppressed IL8 production without affecting cell viability (Figure 1C). The dose responses identified 976 hits that were then binned according to their target hypotheses (hypotheses were assigned on the basis of the known activity of the compounds either from the literature or from previous internal drug discovery programs). The most frequent target hypotheses identified in the screen are shown in Figure 1D. BET family inhibitors were the most numerous in the screen (~7% of the total number of hits). A number of inhibitors targeting proteins previously shown to participate in the IL17A signaling cascade were also identified. These known proteins include PKC family

Figure 2. Overview of the screening strategy and hits from the CRISPR kinome library. (A) Conditions for knocking out genes in primary keratinocytes with CRISPR were optimized by introducing CAS9 and then simultaneously introducing GFP and sgGFP. (B) Conditions for IL8 staining, including stimulation conditions with IL17A/TNF, were optimized, and the staining was tested for inhibition with the tool compound TPCA1. (C) Once conditions were optimized, Cas9 was transduced into primary keratinocytes followed by transduction of 3052 sgRNAs targeting 729 different kinases. Transduced cells were treated with IL17A/TNF to induce IL8 production, and positively stained cells were sorted into three pools: low IL8 staining, high IL8 staining, and the remainder of the cells. (D) Representative histogram from 1000000 cells collected for screening. The total number of cells collected for each population is shown in the table. (E) False discovery rate (FDR) for the kinase library for positive and negative regulators of IL8 staining. The top 15 hits for both categories are shown in the insets.

members, PI3K family members, NFκB-related targets, and heat shock protein 90 (HSP90). As compounds were not equally distributed among all targets in the library, the initial target hypotheses obtained from the screen were also ranked by comparing the number of hits specific for a given target versus the number of compounds against that target in the entire library (Figure 1E). In this analysis, the Gardner–Rasheed feline sarcoma viral oncogene homologue (FGR) and TNNI3 interacting kinase (TNNI3K) were among the top hits. BET family members were the 12th highest, with 52% of the BET family inhibitors recovered from the library.

Second, a pooled CRISPR library targeting 729 kinases was also screened in the same cell-based system. To determine if we could apply Cas9-medated genome-editing technology in human primary adult keratinocytes, we performed a CRISPR reporter assay to measure Cas9 activity. This assay assessed Cas9 activity using lentiviral particles containing GFP and a gRNA against GFP. As shown in Figure 2A, the GFP signal was nearly abolished in the presence of Cas9, indicating that Cas9 effectively exerted its nuclease activity. Extensive optimization was further conducted to maximize intracellular IL8 staining after IL17A/TNF treatment and to prove that IL8 staining could be reduced with a known inhibitor (TPCA1, IKKαβ inhibitor) of IL17A/TNF signaling (Figure 2B). Once optimized, Cas9 and 3052 pooled gRNAs representing 729 kinases were transduced into the cells in succession, and screening was conducted in a pooled format using fluorescence-assisted cell sorting (FACS) (Figure 2C). The

~10% of keratinocytes with the lowest level of IL8 staining, the ~10% with the highest level of staining, and the remaining ~80% were collected into separate pools. These pools were processed for DNA isolation, amplification, sequencing, and ultimately target deconvolution (Figure 2D). Positive regulators of IL17A/TNF signaling (i.e., targets that when knocked out reduced the level of IL8 staining) and negative regulators are shown in Figure 2E. Many of the top positive regulators were known components of the IL17A signaling cascade, namely, CHUK (IKKα), MAP3K7 (TAK1), and IKBKB (IKKβ). Strikingly, TNNI3K was identified as a positive regulator of IL17A/TNF signaling in small molecule screening but as a negative regulator in pooled genomic screening. One potential explanation for these contradictory results is TNNI3K functioning as a regulator of exocytosis. To test this hypothesis, keratinocytes were stimulated with a combination of IL17A and TNF for 24 h in the presence or absence of 1 μM TNNI3K inhibitor (Supplementary Figure 1A), followed by intracellular staining for IL8 and flow cytometry. As expected, TNNI3K inhibition further induced IL8 staining. When the same compound was titrated into keratinocytes stimulated with IL17A/TNF and IL8 was measured in the supernatants, IL8 production was completely inhibited (Supplementary Figure 1B). These results demonstrate that TNNI3K does indeed regulate exocytosis under these conditions, confirming our CRISPR and small molecule screen results.
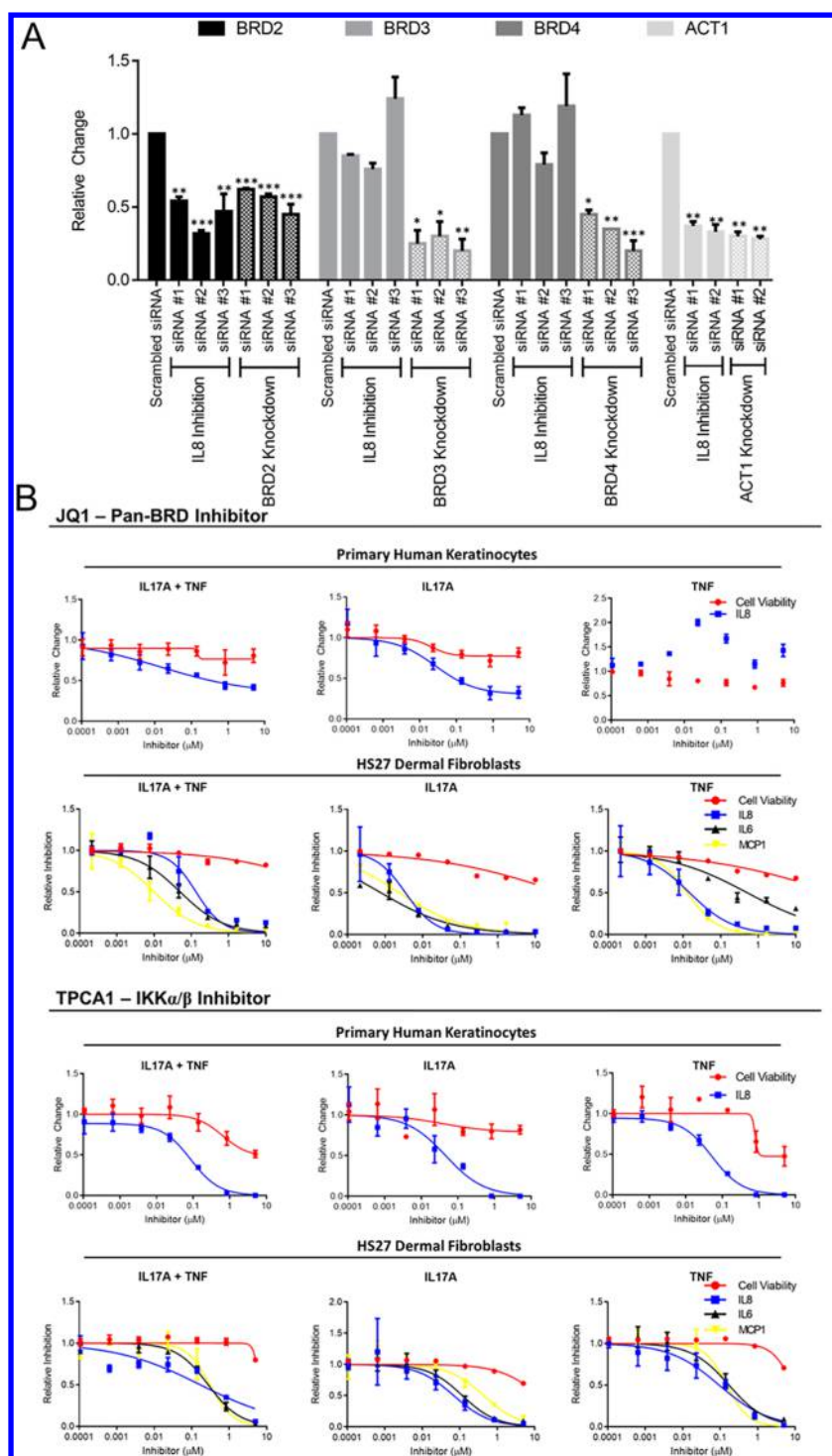
Figure 3. Knockdown of BRDs and pharmacologic inhibition of BRDs in IL17A/TNF-stimulated primary keratinocytes and HS27 fibroblasts. (A) Primary human keratinocytes were transfected with multiple siRNAs targeting BRD2, BRD3, BRD4, and ACT1. Control cells were transfected with an siRNA chemically modified to impair processing and uptake by RISC (RISC-free). After being incubated for 2−3 days, keratinocytes were stimulated with IL17A/TNF for 16 h. Supernatants were collected and assayed for IL8 secretion. BRD and ACT1 knockdown efficiency was measured by real-time qRT-PCR. Data shown represent an average of three replicates. (B) Keratinocytes or HS27 fibroblasts were treated with escalating doses of the pan-BRD inhibitor JQ1 or the IKK$\alpha\beta$ inhibitor TPCA1 and then stimulated with TNF and IL17A, IL17A alone, or TNF alone. Supernatants were harvested 24 h after treatment and assayed for IL8 secretion (keratinocytes) or a combination of IL8, IL6, and MCP1 secretion (HS27). Cell viability was determined by measuring a reduction in Cell Titer Glo luminescence. Data shown represent an average of three replicates.

BRD Family Members Were Implicated in Both Screens and Further Investigated by Pharmacologic Inhibition and siRNA Knockdown. BRD2 was the highest-

ranking novel hit identified in our pooled CRISPR kinome screen. The BET family was also the most frequent target family identified from the small molecule annotated library
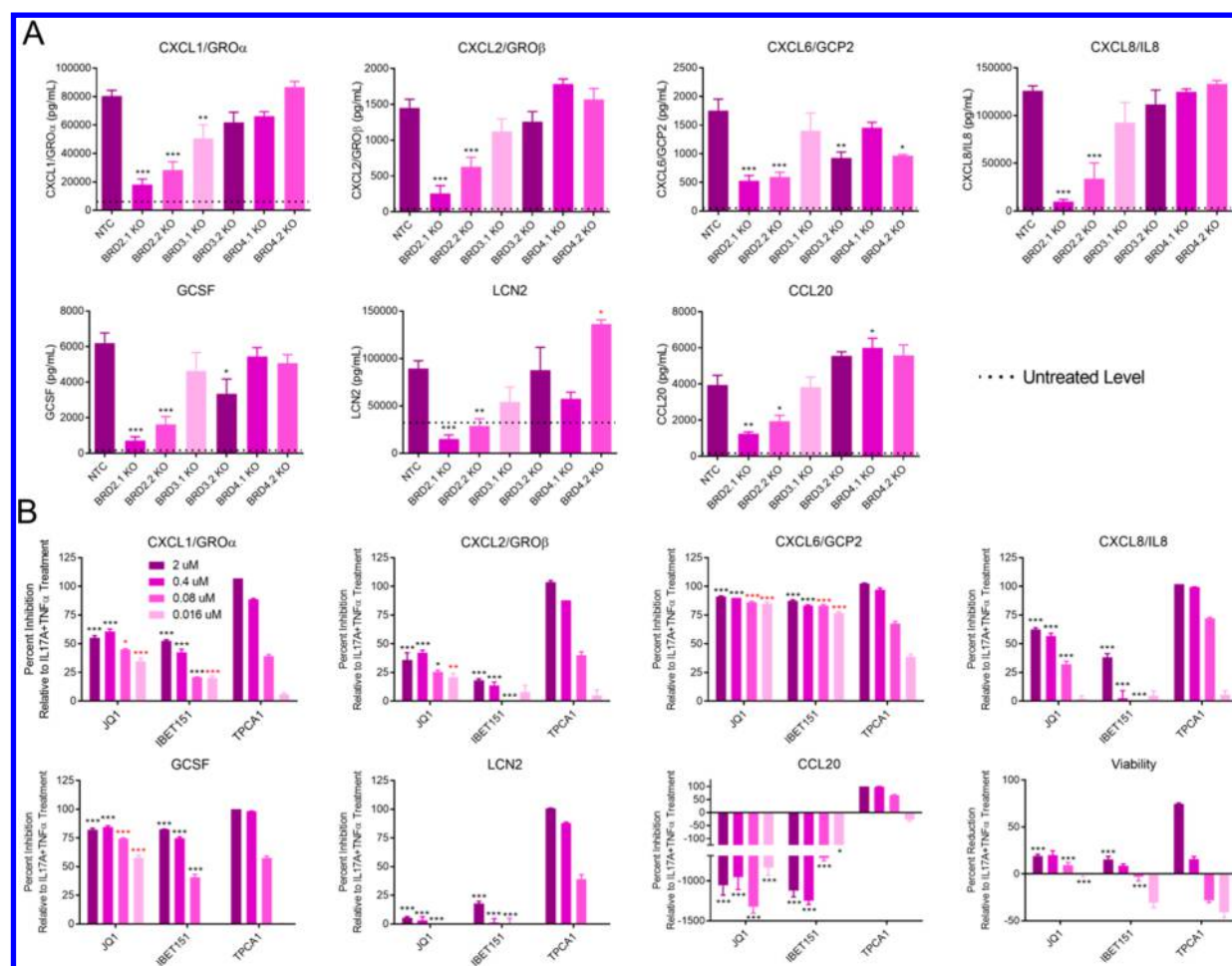
Figure 4. CRISPR knockout and pharmacologic inhibition of BRDs have a unique effect on the secretion profile of IL17A/TNF-stimulated primary keratinocytes. (A) Primary keratinocytes were transduced with a nontargeting control or two unique BRD2/3/4 gRNA sequences (represented as BRD#.1 and BRD#.2). After puromycin selection, transduced cells were stimulated with 200 ng mL^{-1} IL17A and 50 ng mL^{-1} TNF. Supernatants were harvested 24 h after treatment and assayed for CXCL1, CXCL2, CXCL6, CXCL8, GCSF, LCN2, and CCL20. Significant decreases from the NTC group are denoted with black asterisks (***$P < 0.001$, **$P < 0.01$, and *$P < 0.05$), and significant increases are denoted with red asterisks. (B) Comparison of JQ1 and IBET151 (pan-BRD inhibitors) to TPCA1 (IKK$\alpha\beta$) after IL17A/TNF stimulation. Primary keratinocytes were treated with escalating doses of JQ1 and IBET151 or TPCA1 and then stimulated with 50 ng mL^{-1} IL17A and 20 ng mL^{-1} TNF. Supernatants were harvested 48 h after treatment and assayed for the same secreted factors. The cell viability was determined by measuring a reduction in Cell Titer Glo luminescence. Concentrations at which TPCA1 had statistically stronger effects than pan-BRD inhibitors are denoted with black asterisks (***$P < 0.001$, **$P < 0.01$, and *$P < 0.05$), and concentrations at which TPCA1 had weaker effects are denoted with red asterisks. Data shown represent an average of three to four replicates.

screen. However, the particular BET family member(s) involved in IL17A signaling could not be elucidated with small molecule tools (due to a lack of overall selectivity by the compounds available).

To orthogonally validate screening results, the roles of BRDs in IL17A and TNF signaling were further assessed using siRNAs to knock down the three most common BET family members [BRD2, BRD3, and BRD4 (Figure 3A)]. No BRDT expression was detected in primary keratinocytes (data not shown), so this family member was not explored further. BRD2 expression levels were reduced by 48% with siRNAs, and the reduction in BRD2 correlated with a 52% reduction in IL17A/TNF-driven secretion of IL8. The strong correlation between mRNA reduction and IL8 secretion was also recapitulated with siRNAs against ACT1 (a well-known signal transduction partner of IL17 receptors). Notably, BRD3 and BRD4 were knocked down by siRNAs with 75% efficiency, but this did not result in any reduction in IL8 secretion. We attempted to deconvolute the role of BRD2 in IL17A versus TNF signaling

by stimulating keratinocytes with IL17A alone or TNF alone. Unfortunately, we found that neither cytokine alone sufficiently stimulates the production of IL8 from primary keratinocytes after the stress of siRNA transduction or CRISPR knockout (data not shown).

To cross-validate the small molecule screen and deconvolute the role of BRDs in isolated IL17A or TNF signaling, the commercial pan-BRD inhibitors JQ1 and IBET151 were utilized. Although pan-BRD inhibitors are not a direct surrogate for selective knockout of BRD2, given the inability to deconvolute IL17A versus TNF signaling with gene silencing methods, pharmacologic inhibition was the best alternative. JQ1 reduced IL8 secretion by 58% in keratinocytes stimulated with a combination of IL17A and TNF (Figure 3B). Notably, the 58% reduction was similar to the 52% reduction observed with siRNA. When IL17A alone was used to drive IL8 secretion, more robust IL8 inhibition was observed (75%). Strikingly, JQ1 increased TNF-mediated IL8 secretion by 2−3-fold. This observation (BRD inhibition reducing IL17A
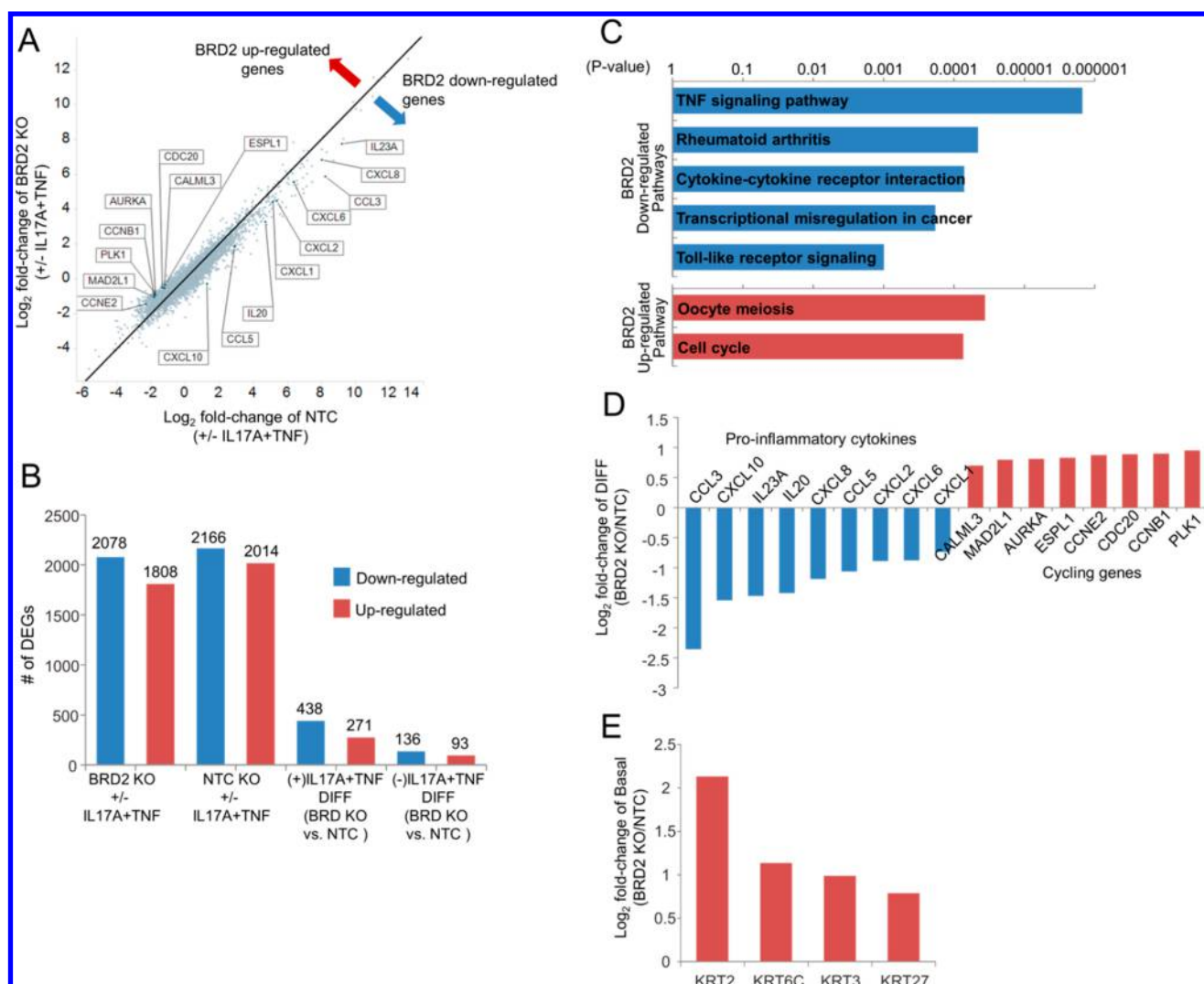
Figure 5. Global gene profiling of NTC and BRD2KO primary keratinocytes. (A) Genomewide overview of a differentially expressed gene after IL17A/TNF treatment in BRD2KO and NTC. "BRD2 downregulated" genes refer to those that decrease with BRD2 KO; "BRD2 upregulated" genes refer to those that increase. (B) Total number of differentially expressed genes (DEGs, $\log_2$ fold change 0.7 cutoff) that are downregulated (blue) or upregulated (red) in the presence (+) or absence (−) of IL17A and TNF in primary keratinocytes. DIFF denotes the total number of DEGs with a 0.7 $\log_2$ fold change in expression between BRD2KO and NTC. (C) Genes derived from DIFF groups were subjected to KEGG pathway enrichment analysis. Pathways with the most significant enrichment ($P < 0.001$) are shown. (D) $\log_2$ fold change in selected BRD2KO downregulated and upregulated genes from the DIFF group. (E) $\log_2$ fold change of keratin gene family members in unstimulated cells.

signaling but increasing TNF) was recapitulated with IBET151 (Supplementary Figure 2). It should be noted that primary keratinocytes stimulated with IL17A or TNF alone secreted ~80% less IL8 (~800 pg mL^{-1} vs ~3300 pg mL^{-1}) than keratinocytes treated with IL17A and TNF together. This suggests that cellular production of IL8 was not saturated and the roughly 2-fold increase we observed is within a meaningful range of induction. To ensure that the increase in IL8 secretion was not an artifact of the cell system, the IKK$\alpha\beta$ inhibitor TPCA1 was also tested across all stimulation conditions. As NFkB signaling is central to both IL17A and TNF stimulation, TPCA1 was expected to completely and dose dependently reduce IL8 secretion across all conditions. The data in Figure 3B confirm the role of NFkB in the system, helping validate the results with pan-BRD inhibitors.

In addition to keratinocytes, dermal fibroblasts are also an important responder to IL17A and TNF signaling in skin. Because bromodomain protein inhibition with small molecules

has been previously shown to affect inflammatory activation and the functional properties of fibroblasts,[24] we utilized HS27 (immortalized dermal fibroblasts) as an alternative *in vitro* model to better understand the effects of BET inhibitors. We tested JQ1 and IBET151 in HS27 dermal fibroblasts for effects on IL17A and TNF stimulation (Figure 3B and Supplementary Figure 2). Notably, IL8 was reduced across all conditions tested, suggesting that BRDs regulate TNF signaling differently between keratinocytes and fibroblasts. To ensure that these effects in fibroblasts were not an artifact of IL8 secretion, both IL6 and monocyte chemoattractant protein 1 (MCP1) were also quantified. Secretion of both factors was completely and dose-dependently reduced regardless of the stimulus (IL17A/ TNF, IL17A, or TNF). The control compound TPCA1 once again dose-dependently reduced IL17A and TNF signaling. Given the differential response between keratinocytes and fibroblasts, we sought to corroborate the pharmacologic inhibition data with a gene silencing technique. Clonal

G
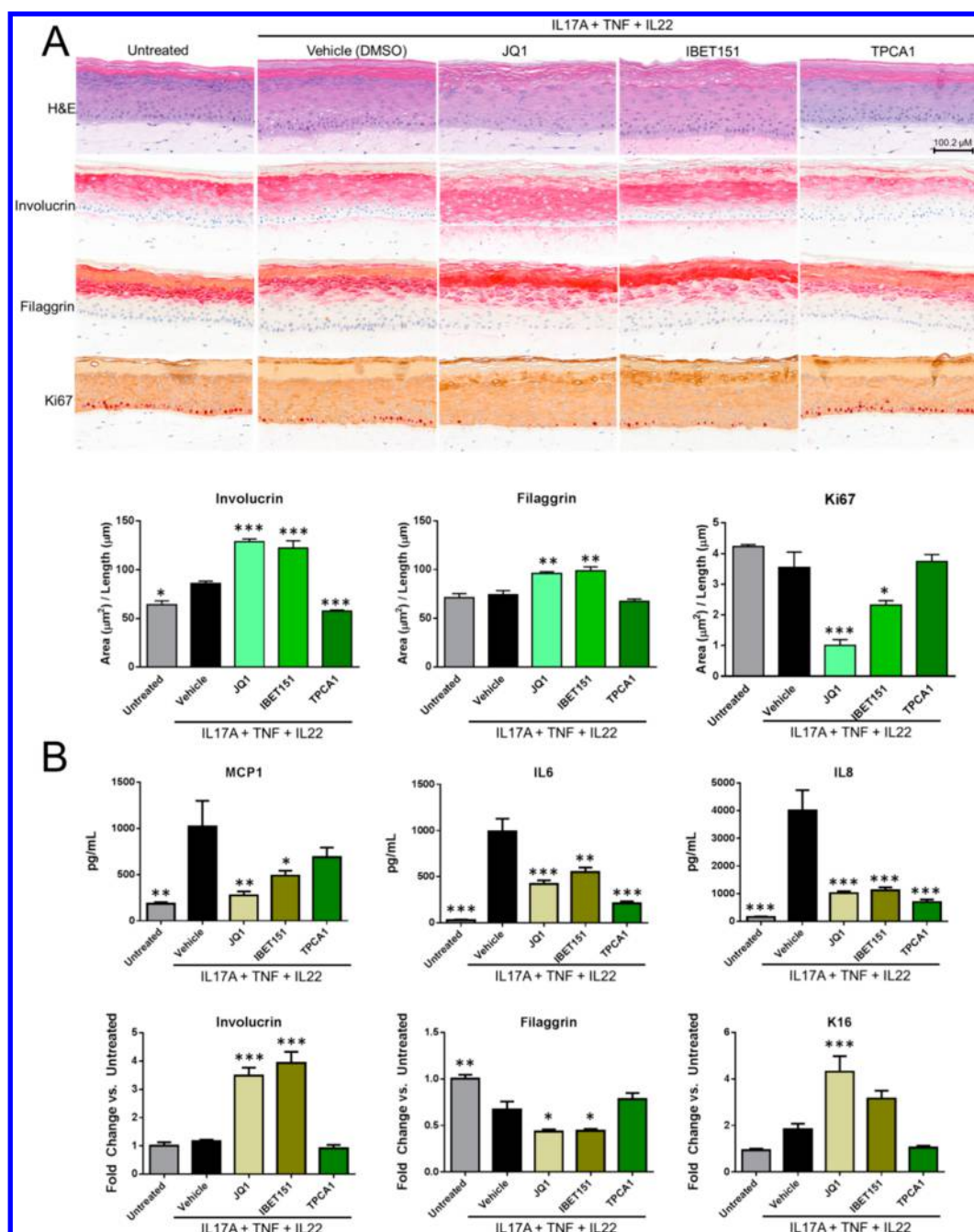
Figure 6. Pharmacologic inhibition of BRDs drives an aberrant cornification profile in 3D organotypic raft cultures *in vitro*. Skin rafts were treated with pan-BRD inhibitors JQ1 and IBET151 or the IKKα/β inhibitor TPCA1 and then stimulated with a combination of TNF, IL17A, and IL22 (all at a final concentration of 1 ng mL^{-1}). (A) After 72 h, a portion of the raft was fixed, sectioned, and used for histology (H&E, involucrin, filaggrin, and Ki67). Representative images at 32× magnification are shown. Quantification of raft histology was captured by analyzing the area of positive involucrin, filaggrin, or Ki67 staining normalized to the length of the raft section. For Ki67, pan-cytokeratin (brown) was used to confine the area of positive Ki67 staining to keratinocytes and to exclude proliferating fibroblasts. (B) Supernatants were harvested 48 h after treatment, and MCP1, IL6, and IL8 were quantified. Another portion of the raft was lysed for qPCR analysis at 72 h (involucrin, filaggrin, and K16). Statistical analysis comparing all conditions to vehicle- and IL17A/TNF/IL22-treated samples was conducted using analysis of variance with Dunnett's post hoc test (***$P < 0.001$, **$P < 0.01$, and *$P < 0.05$).

CRISPR knockouts of BRD2 were generated in HS27s, and BRD2 knockout was verified at the DNA and protein level. HS27 cells retain enough sensitivity to IL17A alone and TNF alone after CRISPR knockout to measure the response to these cytokines independently. Two unique BRD2 knockout clones stimulated with IL17A or TNF had reduced IL8 production, corroborating the phenotype demonstrated by JQ1 and IBET151 (Supplementary Figure 3).

BRD2 Broadly Affects IL17A/TNF Signaling and Keratinocyte Homeostasis. To gain a more comprehensive view of the role that BET family proteins play in IL17A and TNF signaling in keratinocytes, a panel of secreted factors (CXCL1/2/6/8, LCN2, GCSF, and CCL20) and RNA-Seq analysis were utilized. Primary keratinocytes were transduced with CRISPR-Cas9 along with nontargeting controls or BRD2/3/4 gRNA sequences in two biological replicates. As

shown in Figure 4A, BRD2 knockout significantly inhibited IL17A/TNF-mediated secretion of all seven factors tested in the panel by 60% compared to nontargeting controls. Neither BRD3 nor BRD4 inhibited the production of secreted factors in this panel as robustly as BRD2, with most outputs being unaffected or slightly increased. These data suggest that BRD2 plays a larger role beyond IL8 secretion in IL17A/TNF activation of keratinocytes and corroborate the findings for the initial pooled CRISPR screen.

To determine if these findings could be recapitulated by pharmacologic inhibition, both JQ1 and IBET151 were also tested against this secreted factor panel (Figure 4B). Both inhibitors robustly reduced CXCL1/2/6/8 and GCSF secretion. IL8 (CXCL8) secretion was partially inhibited (64%), as found previously. LCN2 showed minimal inhibition with both compounds. CCL20 was potently upregulated ~10-fold in the presence of both compounds. As BRD inhibition is known to arrest the cell cycle and drive cell senescence,[25] this upregulation in CCL20 demonstrates that the reductions observed across the other secreted factors were not due to senescence or cell death (and this is further confirmed by the cell viability data in Figure 4B). Across all of these different outputs, JQ1 was consistently the more potent compound, which parallels their biochemical activities, where JQ1 is roughly 2-fold more effective than IBET151 across all BRDs.[20,21] The IKK$\alpha\beta$ inhibitor TPCA1 was again used as a control in these experiments and dose-dependently inhibited all secreted factors.

To gain a genomewide understanding of the function of BRD2 in the regulation of pro-inflammatory cytokine signaling in human primary keratinocytes, we utilized CRISPR to generate BRD2-deficient (BRD2KO) and -unmodified (non-targeting control, NTC) primary keratinocytes using two unique gRNA sequences tested in three biological replicates (n = 6 total samples). Transduced keratinocytes were stimulated with or without IL17A/TNF, followed by RNA-Seq analysis. Differentially expressed genes (DEGs) from these samples were defined as having 0.7 $\log_2$ fold change differences in expression. Using this cutoff, ~2000 IL17A/TNF sensitive DEGs were identified in both BRD2KO and NTC keratinocytes (Figure 5A,B). Within these DEGs, a total of 438 genes showed reduced responsiveness to IL17A/TNF stimulation in BRD2KO keratinocytes (Supplementary Table 2), while 271 had enhanced responsiveness [Figure 5B, (+)IL17A+TNF, and Supplementary Table 3]. To better define the signaling pathways affected by BRD2, KEGG analysis of genes with reduced or enhanced responsiveness to IL17A/TNF in BRD2KO keratinocytes was conducted (Supplementary Table 4). Analysis of genes with reduced responsiveness to IL17A/TNF yielded many statistically significant inflammatory pathways (P < 0.001), including "TNF signaling" pathways and "rheumatoid arthritis" pathways (Figure 5C). These findings are consistent with BRD2 playing a role in IL17A and TNF signaling and corroborate the secreted factor data presented above. Analysis of genes with enhanced responsiveness after BRD2KO yielded significantly fewer pathways of interest. "Oocyte meiosis" and "cell cycle" pathways were the only two statistically significant pathways attributed to this gene set, and both were already known to be BRD2-mediated.[26,27] Interestingly, comparison of unstimulated BRD2KO keratinocytes with NTC keratinocytes revealed a total of 93 DEGs that included a number of genes associated with keratinocyte differentiation, including keratins 2, 6C, 3,

and 27 (KRT2, KRT6C, KRT3, and KRT27, respectively) (Figure 5E).[28−30] Additional genes associated with keratinocyte differentiation, including involucrin (IVL) and filaggrin (FLG), were also affected, but these did not meet our 0.7 $\log_2$ fold change cutoff. Given this bias toward keratinocyte differentiation, we may have expected to see a reduction in expression of genes associated with keratinocyte activation. However, genes associated with activation, including keratins 5, 14, and 16 (KRT5, KRT14, and KRT16, respectively),[28] were all unchanged or marginally increased. These data suggest that knockout of BRD2 drives an aberrant cornification profile in keratinocytes affecting their normal process of differentiation.

Characterization of BRD Inhibition in 3D Organotypic Raft Cultures. To better understand the role of BRD2 in keratinocyte differentiation, 3D organotypic raft cultures were utilized. These 3D cultures allow for the simultaneous quantification of inflammatory factor production as well as structural changes in the raft consistent with changes in keratinocyte differentiation. Rafts were constructed in culture from a layer of human fibroblasts (embedded in collagen to approximate the dermis) and were then seeded with human keratinocytes to recapitulate the epidermal layers in culture. Skin rafts were then treated with a combination of IL17A, TNF, and IL22 to drive histopathologic changes and inflammatory features qualitatively similar to those of human psoriatic plaques (Figure 6). Unfortunately, gene knockout in these rafts is difficult as virally transduced and selected keratinocytes will not form the multilayer architecture required to establish a liquid−air interface (unpublished results). Given this limitation, we again utilized the pan-BRD inhibitors JQ1 and IBET151. As established earlier, these inhibitors reconstitute most (though not all) of the BRD2 knockout phenotype. Addition of IL17A, TNF, and IL22 induced modest keratinocyte vacuolization, marked loss of the keratohyalin granules (hypogranulosis), and a disorganized keratinocyte stratification of the spinosum/granulosum layers (indicating potential defects in differentiation) while maintaining a well-organized basal cell layer when compared to untreated samples (Figure 6A). IL17A, TNF, and IL22 increased the production of the pro-inflammatory factor from the rafts [as measured by IL6, IL8, and MCP1 (Figure 6B)]. Differences in keratinocyte differentiation were quantified by IHC and qPCR of the late differentiation markers involucrin (increased by IHC) and filaggrin (increased by qPCR). Changes in keratinocyte activation were quantified using Ki67 IHC staining and K16 transcript expression. Pan-BRD inhibition significantly reduced proinflammatory factor production (Figure 6B), consistent with 2D keratinocyte culture. Pan-BRD inhibition also drove an aberrant cornification pattern (Figure 6A,B). Involucrin staining and transcript levels were significantly increased upon BRD inhibition. Filaggrin staining was also significantly increased overall, although the increases in filaggrin staining were largely sequestered to the stratum corneum. In the granulosum cell layers, filaggrin staining and transcript levels were decreased. Both BRD inhibitors also induced K16 mRNA expression above those observed with the IL17A/TNF/IL22 treatment, suggestive of increased keratinocyte activation. However, both inhibitors had diminished Ki67 staining by IHC, suggesting a reduction in overall cell proliferation. Taken together these findings corroborate the 2D findings in terms of both the inflammatory response and the aberrant cornification phenotype. Notably,

the IKK$\alpha\beta$ inhibitor reduced inflammatory factor production and, in contrast to BRD inhibition, stabilized the proliferation, differentiation, and cornification profile, establishing the validity of the 3D system.

Selection of a Phenotypic Screening System and Overall Output. The detailed configuration of our assays was chosen to balance high clinical relevance while simultaneously casting a wide net to maximize the target/signaling space covered. We selected IL8 as the primary end point, because it can be upregulated by several parallel pathways downstream from IL17A and is crucial in multiple subsequent processes such as neutrophil recruitment.[31,32] Choosing such a universal readout enabled the screen to capture a broad set of IL17A-mediated signaling events while also maximizing the sensitivity of our screens. We used TNF together with IL17A to stimulate keratinocytes to model additional synergistic IL17A-driven events in our system. That is, TNF activates the transcription of a pool of pro-inflammatory mRNAs that subsequently undergo IL17A-dependent stabilization.[33] Because of the proven clinical efficacy of anti-TNF biologics in treating psoriasis,[5] TNF was selected over other cytokines such as IL1β and IFNγ that have also been shown to synergize with IL17A.[34,35] Deconvoluting IL17A-specific and TNF-specific targets was accomplished downstream in our screening process by using IL17A alone or TNF alone (as independent stimuli) on keratinocytes. This analysis allowed us to ascertain which mode of cytokine signaling (IL17A or TNF) was affected within these complex, combinational signaling cascades (and in some cases, it was both).

Although we considered immortalized keratinocyte cell lines like HaCaTs[36] or other IL17-responsive cell lines like HeLa or HS27 fibroblasts for use in IL17 phenotypic screening, we found that primary keratinocytes robustly respond to IL17A and TNF, producing a number of pro-inflammatory cytokines, chemokines, and growth factors.[33] Additionally, we noted that keratinocytes hyperproliferate in the presence of IL17A, which is a key feature for these cells in the pathogenesis of psoriasis.[8,14] While utilizing primary human cells made the diseased tissue of interest strongly relevant for psoriasis, using these cells for our screens incurred a number of challenges. For example, it is known that primary keratinocytes become senescent under stress, such as viral infection or chronic exposure to inflammatory stimuli.[37,38] Therefore, in the small molecule screen, we had to restrict the cell passage number to only four passages to provide a sufficient signal-to-noise ratio and enable the overall reproducibility needed to obtain useful data. In our pooled CRISPR screen, we found that a high lentiviral titer and short exposure to virus was required to efficiently transduce the cells while minimizing adverse effects. Furthermore, after antibiotic selection, we determined that a resting period of up to 1 week was required before they would resume growth. Despite these challenges, we believe that primary keratinocytes (the most relevant cell type for this phenotypic screening effort) were the best choice for this effort. To the best of our knowledge, no pooled CRISPR screen has been conducted in primary adult keratinocytes prior to this report, although one shRNA screen using neonatal keratinocyte cells was recently published.[39]

The CRISPR screen returned several previously known targets in the IL17A signaling cascade, namely, CHUK (IKKα), MAP3K7 (TAK1), and IKBKB (IKKβ). This provided strong confirmation of the accuracy of our assay system and the relevance of additional targets that it identified.

Two of the unique targets suggested as positive regulators of IL17A signaling by our screen were BRD2 and ULK1. The false discovery rate (FDR) for ULK1 was quite high (0.82), and as such, we did not consider that target for further analysis. In contrast, in the early triage of the screening hits, we found BRD2 to be particularly intriguing due to its low FDR (0.006) and known role in inflammatory signaling.[40] Notably, while BRD3, BRD4, and BRDT guide RNAs were included in the sgRNA library used, none of these other BRD family members emerged as hits in our pooled CRISPR screen. To date, there has been no report in the literature linking BRD2 or the BRD family to IL17A downstream signaling. However, there are multiple reports linking the BRD family to the production of IL17A from TH17 cells,[19,41] which produce IL17A that can subsequently act on recipient cells such as keratinocytes.

Our small molecule screen yielded more total hits (976) than the CRISPR kinome screen. This is perhaps not unexpected due to the larger library size as well as the greater specificity of gRNAs compared to that of small molecule inhibitors, which can often impact multiple targets. To deconvolute the potential mechanisms at work from the hit molecules, we took advantage of the compound annotation within our library. These annotations often enabled a quick translation from chemical matter hit to putative target (that compound structure or pharmacophore similarity analyses could not), and it also provided a more direct comparison between the results of the two screens. Unfortunately, due to the known promiscuity of some hit compounds, exact targets could not be easily assigned for some compounds and had to be approximated to a protein family (such as the BET or PI3K family). In spite of this limitation, a number of molecules targeting proteins previously known to be important for these signaling pathways such as MAP3K7 (TAK1), HSP90, CHUK (IKKα), and PI3K were identified in the annotated library screen, giving additional confidence to the relevance and reliability of the experiments. Interestingly, when ranking targets by the total number of associated hits emerging from the small molecule screen, we found a number of previously unknown targets that altered IL17A/TNF signaling in keratinocytes became evident. The BET family was the highest-ranking hit by this analysis. Other new hits of interest include erb-b2 receptor tyrosine kinase 3 (ERBB3), ribosomal protein S6 kinase A6 (RPS6KA6), TAOK1, HCK, and PAK1.

Of course, prioritizing target hypotheses purely based on the number of associated compounds that were positive in the screen could create unintentional biases depending on the population of compounds against a given target within the library. Thus, we also examined the hit set by comparing the fraction of hits recovered relative to the number of compounds associated with a given target in the library (i.e., hit recovery rate). Using this scheme, the hits with the highest recovery rate were FGR, TNNI3K, EPH receptor A6 (EPHA6), and the PKC family while the BRD family was somewhat less emphasized in this analysis. FGR and TNNI3K are novel hits that have no previously known involvement in the IL17A signaling cascade. We also found that EPHA6 was ranked third in this analysis. Interestingly, while our data suggest a role for EPHA6 in IL17A signaling, a closely related family member, EPHA2, has been shown to be upregulated in psoriatic epidermis.[42] We also note that the PKC family, which is known to participate in IL17A signaling,[43] was a frequent hit.

Small molecule inhibitors targeting bromodomains, such as JQ1 and IBET151, hinder binding of BET protein to

acetylated lysines but lack selectivity within the BET family (BRD2/3/4), making it difficult to untangle contributions of each family member to transcriptional and cellular outcomes.[44,45] Thus, one of the goals for this CRISPR kinome screen was to build a more specific link between BET proteins and IL17A signaling by interrogating each of the individual BET family members and assessing their impact on the IL17A pathway. Interestingly, our screen results demonstrated that all gRNAs against BRD2 [four of four (Supplementary Figure 4)] were enriched for IL8 positive regulators, suggesting that BRD2 has a profound impact on IL17A- and TNF-stimulated IL8 production in disease relevant human primary keratinocytes. Although we cannot completely rule out the involvement of BRD3 and BRD4 in the IL17A/TNF pathways in keratinocytes, our chemical and genetic screen data suggest that the therapeutic effect of current pan-BRD inhibitors most likely acts through BRD2 rather than BRD3 and BRD4. Furthermore, it would be sensible to synthesize BRD2-specific small molecules to more precisely modulate BRD2, although we note the challenges of obtaining such molecules may be considerable.

Role of BRD2 in IL17A/TNF Signaling and Keratinocyte Differentiation. Human skin and its immune cells provide the first line of defense against microbial pathogens as well as physical and chemical insults. Indeed, recent studies underscore the significance of keratinocytes as immune sentinels, nonprofessional antigen-presenting cells, inducers of inflammation, and producers of innate immune mediators.[46] BET family proteins exert their enzymatic, protein recruitment, and histone modification activities via lysine acetylation, revealing an array of mechanisms involved in transcriptional regulation and chromatin remodeling. Thus, inhibition of BET family proteins has been shown to be a promising approach not only for anticancer therapy but also for treating chronic inflammatory diseases.[12,40,47] However, the ability of BET proteins to coordinate the response of inflammatory cytokine genes in human primary keratinocytes is largely unknown.

Given the potential for false positives in screening, one goal of this study was to comprehensively verify the role of BRD2 in IL17A signaling utilizing a number of orthogonal methods. Both siRNA and CRISPR knockout of BRD2 in primary keratinocytes as well as clonal CRISPR knockout of BRD2 in HS27 dermal fibroblasts indicated that BRD2 plays a role in IL17A and TNF signaling. Moreover, treatment of primary keratinocytes and HS27 dermal fibroblasts with two pan-BRD inhibitors also corroborated the gene silencing and genetic knockout results. Another possible disadvantage of running high-throughput screens with a single output is the potential to identify peripheral signaling nodes in a pathway that regulates only a small number of downstream genes rather than central signaling nodes controlling a larger number of genes. BRD2 knockout and pan-BRD inhibition with small molecule compounds both robustly blocked the secretion of a number of different inflammatory factors (eight of eight and six of eight factors, respectively). It is unclear why BRD2 knockout had a stronger effect in this secreted factor panel, although the high specificity of CRISPR reagents compared to the pan-BRD profile of the compounds is one possibility. In this scenario, BRD3 or BRD4 inhibition would compensate and reverse the effects of BRD2 inhibition for certain genes. Another possibility is the pleiotropic role of BRD2 in signaling. The small molecule compounds can neutralize only the histone binding activity of BRD2, while CRISPR knockout will also

eliminate its scaffolding and kinase activity. To better answer this question, we attempted to reconstitute kinase dead or histone binding dead mutants of BRD2 in clonal HS27 BRD2KO cells. However, restoration of IL17A/TNF signaling in these cells was unsuccessful. Briefly, BRD2 reconstitution was accomplished by lentiviral transduction with a vector encoding GFP-tagged BRD2. Visualization of intracellular protein levels by immunoblotting confirmed efficient expression of GFP-BRD2. However, constitutive expression of the GFP-BRD2 construct did not potentiate IL8 cytokine release in BRD2KO cells. To rule out interference by the GFP tag with exogenous BRD2 protein function, we tested several additional lentiviral constructs encoding FLAG-tagged or untagged BRD2. Despite efficient infection of target cells with the new lentiviral constructs, phenotypic rescue was not observed. Immunostaining of cellular lysates showed that both FLAG-tagged and untagged BRD2 were poorly expressed at the protein level (data not shown). There are several potential explanations for the failure of these experiments, including isoform differences (five endogenous transcript variants, but only one variant tested here), a lack of appropriate subcellular localization, or a lack of stability of the protein constructs.

In addition to the secreted factor panel, RNA-Seq experiments were utilized to gain a genomewide view of IL17A/TNF signaling in BRD2-deficient keratinocytes. A total of 709 genes (438 suppressed and 271 enhanced) were differentially regulated in BRD-deficient keratinocytes after IL17A/TNF stimulation. Notably, the 438 suppressed genes were clustered into a number of pro-inflammatory pathways, consistent with the known role of BRD2 in inflammation.[23,25,40] The genes with enhanced sensitivity were not well represented in many known pathways. The two most highly significant hits determined by KEGG analysis ("oocyte meiosis" and "cell cycle") both have been attributed to BRD2 previously.[26,27] However, the majority of genes in this set were not attributed to known pathways, suggesting some unique and underexplored biology may be present. Collectively, given the total number of genes whose expression is altered, these changes indicate that BRD2 plays more than a peripheral role in IL17A and TNF signaling. We do note that the magnitude of the fold change for most differentially expressed genes was relatively small (~2−4-fold), although the impact could likely be increased by adjusting IL17A/TNF concentrations and/or kinetics.

RNA-Seq analysis of unstimulated keratinocytes also revealed a number of interesting changes in keratinocyte differentiation. Keratinocyte differentiation (also known as cornification) is the process by which keratinocytes undergo apoptosis to produce tough protective layers and/or structures in the skin. Numerous differentiation markers have been identified, including both early (KRT1 and KRT10) and late (FLG and IVL) markers. Undifferentiated or activated keratinocyte markers (KRT5, KRT14, and KRT16) have also been described (reviewed by Eckhart et al.[28]). In a normal differentiating keratinocyte, activation markers should gradually decrease while differentiation markers increase over a keratinocyte's life span. Strikingly, in BRD2-deficient keratinocytes, the differentiation markers increased but the activation markers did not substantially decrease. This profile suggests that BRD2 deficiency can drive aberrant cornification (which was also seen with pan-BRD small molecules). This is an intriguing finding as effects on cell cornification is a common theme in many studies of skin diseases.[29,48,49]

Given the limitations of 2D culture, we also sought to determine the role of BRD2 in 3D organotypic raft cultures. This model provides a way to measure inflammatory factor production driven by IL17A, TNF, and IL22 and keratinocyte proliferation, stratification, differentiation, and cornification within a recapitulated skin relevant 3D structure.[9] As mentioned previously, assembly of the skin rafts requires unperturbed (genetically or chemically) keratinocytes. As such, pan-BRD inhibitors were used for this study. As expected, the inhibitors neutralized inflammatory factor production, including IL8, IL6, and MCP1 secretion. Taken together with the RNA-Seq data and secreted factor data, these findings provide strong evidence of a role of BRD2 in IL17A/TNF-dependent skin inflammation. Moreover, the BRD inhibitors also produced an aberrant cornification profile consistent with the RNA-Seq data. Two markers of the cornified envelope (involucrin and filaggrin[9]) were differentially affected by BRD inhibition. Involucrin, which is significantly upregulated by IL17A, TNF, and IL22, was further upregulated by BRD inhibition at the protein and mRNA level. Filaggrin expression, which was unchanged by IL17A, TNF, and IL22 at the protein level and decreased at the transcript level, was robustly upregulated by BRD inhibition in the stratum corneum of the raft cultures leading to an overall increase in staining. However, filaggrin staining appeared weaker in granular keratinocytes, and this decrease in staining was corroborated by qPCR, which showed a decrease in filaggrin transcripts (beyond the decrease mediated by IL17A, TNF, and IL22). Additionally, KRT16, a marker of keratinocyte activation, was increased while Ki67, a general marker of proliferation, was decreased. While KRT16 and Ki67 are not necessarily expected to correlate (as they measure different aspects of cell proliferation), seeing them dysregulated is another example of aberrant cornification in our current studies. As BRD2 deficiency in 2D culture was sufficient to drive aberrant cornification, we also asked if pan-BRD inhibition alone could mediate aberrant cornification in 3D culture. Indeed, as shown in Supplementary Figure 5, pan-BRD inhibition mediated many of the same changes (dysregulation of Ki67 and KRT16 and increased involucrin staining).

Overall, the studies described here demonstrate that BRD2 is a unique modulator of IL17A signaling. This finding emerged from two separate phenotypic screens carried out in primary keratinocytes that identified BRD2 as a component of the IL17A signaling cascade (Supplementary Figure 6). Genomewide analysis in BRD2-deficient keratinocytes suggests that BRD2 plays a distinct role in IL17A and TNF signaling as well as in keratinocyte differentiation. These results were recapitulated in 2D and 3D cell models. Collectively, the work presented here demonstrates a novel role for BRD2 with the potential to motivate additional work in drug discovery in the IL17/TNF pathways. If BRD2 can be modulated in the skin in a manner sufficiently safe for psoriasis patients, it could offer new therapies for the treatment of this significant disease.

■ METHODS

Chemicals. All reagents were purchased from Sigma-Aldrich unless otherwise specified.

Cell Culture. Primary normal human epidermal keratinocytes (NHEKs) were purchased from Life Technologies and maintained in Epilife Medium (Life Technologies) with the HKGS Kit (Life Technologies), unless otherwise specified. HS27 dermal fibroblasts were obtained from ATCC and maintained in DMEM (Life Technologies) with 10% (v/v) FBS (Life Technologies) and 1% (v/v) penicillin/streptomycin (Life Technologies). All cells were lifted with TrypLE (Life Technologies) and neutralized with a trypsin neutralization solution (Life Technologies). All cells were grown in a humidified atmosphere with 5% CO_2 at 37 °C.

TaqMan Probes for Real-Time PCR. TaqMan probes for 3D organotypic raft cultures from primary human keratinocytes and individual siRNA validation were purchased from Applied Biosystems: K16, Hs00955088_g1; involucrin, Hs00846307_s1; filaggrin, Hs00856927_g1; RPLP0, Hs99999902_m1; GAPDH, Hs99999905_m1; Act1, Hs00974570_m1; BRD2, Hs01121986_g1; BRD3, Hs00978980_m1; BRD4, Hs04188087_m1.

siRNA Constructs. All siRNA constructs were purchased from Dharmacon: negative control, siGENOME RISC-free control (catalog no. D-001220-01); Act1, siGENOME human Act1, catalog no. D-004311-02 (siRNA #1), catalog no. D-004311-03 (siRNA #2); BRD2, siGENOME human BRD2, catalog no. D-004935-01 (siRNA #1), catalog no. D-004935-04 (siRNA #2), catalog no. D-004935-18 (siRNA #3); BRD3, siGENOME human BRD3, catalog no. D-004936-02 (siRNA #1), catalog no. D-004936-03 (siRNA #2), catalog no. D-004936-17 (siRNA #3); BRD4, siGENOME human BRD4, catalog no. D-004937-03 (siRNA #1), catalog no. D-004937-04 (siRNA #2), catalog no. D-004937-05 (siRNA #3).

Statistics. GraphPad Prism was used to generate graphs and perform statistical analyses. Where appropriate, a one-way analysis of variance with Dunnett's test was performed post hoc to assess significant differences (*$P < 0.05$, **$P < 0.01$, and ***$P < 0.001$). Error bars depict standard errors of the mean unless otherwise specified.

High-Throughput Small Molecule Screen. NHEKs were maintained in EpiLife Medium with the HKGS Kit to a passage number of ≤5 and to a confluency of ≤90%. For plating, cells were dissociated with TrypLE, mixed in a 1:1 ratio with trypsin neutralizing solution, centrifuged at 150g, and plated at a density of 2500 cells per well in 384-well tissue culture plates in the medium described above without hydrocortisone. After overnight growth, the medium was removed, and the appropriate concentration of dimethyl sulfoxide-dissolved compound was diluted in plating medium in a separate 384-well polypropylene plate and transferred to the empty cell plate via Biomek FX (Beckman Coulter) to produce the desired final compound concentration. Cells were incubated for at least 30 min in the presence of compounds, and then human IL17A and TNF were added to produce final concentrations of 150 and 60 ng mL^{-1}, respectively. Plates were incubated overnight, and 8 μL of supernatant was transferred to a small-volume 384-well plate. Testing for IL8 (Cisbio) and CXCL1 (Cisbio) was performed using homogeneous time-resolved fluorescence (HTRF) kits according to the manufacturer's instructions. The screen was run from a single copy of the compound library, with selected picks tested in concentration response format. Z′ values were calculated from in-plate control wells (six positive and six negative). The average Z′ for the screen was 0.68 ± 0.14 (standard deviation of the mean).

FACS-Based CRISPR Genomic Screen. SpCas9 lentiviral particles and the Brunello kinome CRISPR library (729 kinase genes representing 3052 sgRNAs) were obtained from the Broad Institute (https://www.broadinstitute.org/genetic-perturbation-platform).

While the life span of NHEKs is finite (limited to a small number of cell divisions) and variability is found among donors or passage number, we carefully monitored cell properties to ensure our two-step CRISPR transduction stayed within culturing-time (~30 days) and passage number (5 passages) limits. Briefly, 20 million NHEKs were infected with Cas9 lentivirus (week 0, passage 1) that were previously thawed from frozen stocks. Cas9-transduced NHEKs were subjected to blasticidin selection (4 μg mL^{-1}). After the NHEKs had recovered from selection (week 1, passage 2), we propagated Cas9 knock-in NHEKs in preparation for screening (week 2, passages 3 and 4). Finally, 40 million NHEKs were infected with guide RNAs from the Brunello Kinome library, followed by puromycin selection (4 μg mL^{-1}) and recovery from selection (weeks 3 and 4, passages 4 and 5).

Prior to flow sorting, lentivirally transduced cells were treated with IL17A (200 ng mL^{-1}) and TNF (50 ng mL^{-1}) for 2 days.

The infection efficiencies for CAS9 and guide RNA transduction were 38% and 32%, respectively, as measured by inline infection Cell Titer Glo (Promega) assays. The cell yield after IL17A/TNF treatment and trypsinization was ~30% (12 million vs 40 million expected). Cells were sorted into three bins using AriaFusion. A total of 0.59, 0.59, and 4.2 million cells were recovered from IL-8 low, high, and middle groups, respectively, to yield 0.62, 1.0, and 2.3 μg of genomic DNA, respectively. Overall, these numbers were significantly lower than expected by several-fold and reflect various technical challenges associated with the delivery of Cas9 into primary cells, intracellular cytokine staining and cell sorting, and preparation of genomic DNA from paraformaldehyde-fixed cells.

On the day of sorting, doubly transduced cells were treated with a protein transport inhibitor cocktail (eBioscience) for 3 h. Approximately 40 million cells were harvested and resuspended in cold phosphate-buffered saline (PBS). We stained the transport-inhibited cells with zombie violet (Biolegend), followed by 0.5% PFA fixation (Alfa Aesar). After being washed with 1× PBS with 5% human serum (Sigma), cells were resuspended in 1× BD Biosciences Perm/Wash Buffer and stained with anti-human IL8-APC (eBioscience catalog no. 17-8088-42).

Fluorescence-based cell sorting (FACS) was performed on a FACSAria Fusion sorter (BD Biosciences) using standard 100 μm nozzle settings. Scatter signals from the 488 nm laser as well as Zombie Violet (BioLegend) and IL8 APC (eBioscience) fluorescence signals were captured. The APC detector (660/20 BP filter) and Pacific blue detector (450/50 BP filter) voltages were determined using untreated NHEKs. Live cells were gated by drawing a region around low Zombie Violet fluorescence, and single cells were targeted using forward scatter area and height pulse processing. Lastly, the top 10% (IL8 high), bottom 10% (IL8 low), and remaining 80% (IL8 remaining) of the IL8 APC signal were gated using an APC histogram and set to be sorted into three collection tubes. The total event rate (1000−2000 events per second) was optimized to achieve the greatest yield while maintaining high purity (>95%).

After genomic DNA isolation using Zymo Genomic DNA Kits, 28 cycles of PCR were performed for all three groups (IL-8 low, IL-8 high, and IL-8 remaining) and plasmid control to amplify the region of interest following the protocol from the Broad Institute's Genetic Perturbation Platform [PCR of sgRNAs, shRNAs, and ORFs from genomic DNA for Illumina sequencing (https://www.broadinstitute.org/genetic-perturbation-platform)]. After PCR, each Illumina-adapted amplicon product was purified using SPRI select beads (Beckman Coulter) and brought to 4 nM prior to being pooled for sequencing on an Illumina NextSeq500 instrument using an Illumina high-output v2 75 cycle kit (Illumina). Altogether, 44 million, 55 million, 51 million, and 88 million postfiltered (PF) reads were generated for IL8 low, IL8 high, IL8 remaining, and plasmid control, respectively.

Following next-generation sequencing (NGS) deconvolution and initial QC, data have been further analyzed to understand global characteristics of screening results. Briefly, one biological replicate of IL8 high, IL8 low, and IL8 remaining was collected and subjected to NGS (four technical/sequencing replicates per each group). The kinome barcode histogram showed a narrow distribution (no runaway or absent gRNAs) throughout 12 lanes (Supplementary Figure 6). In addition, a pairwise comparison between technical replicates was nearly identical ($R > 0.99$), indicating a successful NGS execution (data not shown). The accumulated kinome library within a 6-fold range was 92% (IL8 remaining), 90% (IL8 high), and 81% (IL8 low), revealing a significant reduction in library representation, especially in low versus remaining bins (Supplementary Figures 7 and 8). As a result, true positives might be highly enriched in a smaller sampling bin (IL8 low).

After the demultiplexing of reads (bcl2fastq, Illumina), quantification of sgRNA across all samples was done with a custom Perl script (available upon request). Briefly, users specify the location of the read containing the sgRNA or the flanking primer sequence (if the sgRNA

position is not constant in all reads). Sequences between the flanking sequences or by location were extracted and compared to a database of sgRNA for a library. Only perfectly matched reads were kept and used in the generation of the count matrix. TMM normalization and scaling to CPM were performed across all samples using the edgeR Bioconductor package. Hit selection for the primary screen was carried out using model-based algorithm MAGeCK.[50] The low (1%) cohort was compared to the remaining (95%) cohort where membership denotes the IL8 expression level. The FDR and MAGeCK rank from the MAGeCK analysis shown in Figure 2 are at the gene level.

Individual siRNA Validation (HTRF and qRT-PCR assays). NHEKs were cultured in serum-free keratinocyte growth medium (Lonza) for two or three passages. The cells were reverse transfected with small interfering RNAs (siRNAs) as follows. First, both the siRNAs (Dharmacon) and the RNAiMAX transfection reagent (Life Technologies) were diluted in Opti-MEM reduced serum medium (Life Technologies). Second, the diluted siRNAs were combined with the diluted transfection reagent and incubated for 30 min at room temperature. During the incubation period, cells were dissociated with trypsin-EDTA (Life Technologies), mixed with a trypsin neutralizing solution (Life Technologies), and sedimented by centrifugation. The supernatant was discarded, and cells were resuspended in fresh growth medium, mixed with siRNA/transfection reagent complexes, and seeded into six-well dishes. The medium was replaced 2−3 days post-transfection, and the cells were treated with a combination of 50 ng mL^{-1} IL17A and 20 ng mL^{-1} TNF.

Cell supernatants were collected 16 h post-treatment and assayed with a human IL8 detection kit (Cisbio) by HTRF. To measure siRNA-mediated silencing of gene expression, cells were washed once with DPBS (Life Technologies) and total RNA isolated with the RNeasy Mini Kit (Qiagen) per the manufacturer's instructions, including the on-column DNase treatment step (Qiagen). RNA samples were assayed with the RNA-to-CT one-step kit (Applied Biosystems) by real-time qRT-PCR using TaqMan probes. To calculate knockdown efficiency, mRNA levels in knockdown cells were normalized to those in control cells. GAPDH was utilized as an endogenous reference gene.

Pharmacological Inhibition Validation. NHEKs were cultured in Epilife Medium with the HKGS kit and plated at a density of 10000 cells per well in 96-well plates. After incubation for 24 h, the medium was replaced with hydrocortisone-free growth medium and compounds (JQ1, IBET151, or TPCA1) were added to the plates. Following a 30 min preincubation with compounds, IL17A (50 ng mL^{-1}) and TNF (20 ng mL^{-1}) were added to the plates for 24 h. Supernatants were harvested, and IL8 levels were quantified using kits from Cisbio following the manufacturer's instructions. To the remaining cell layers was added Cell Titer Glo (Promega) for 30 min, and luminescence was quantified using a PerkinElmer Microbeta instrument. Data were analyzed in GraphPad Prism. A total of three keratinocyte donors were tested.

HS27s were cultured in DMEM with 10% (v/v) FBS and 1% (v/v) penicillin/streptomycin. Cells were plated at a density of 7500 cells per well in 96-well plates. After 24 h, the medium was replaced with fresh medium and compounds (JQ1, IBET151, or TPCA1) were added. Following a 30 min preincubation with compounds, IL17A (50 ng mL^{-1}) and TNF (20 ng mL^{-1}) were added to the plates for 16 h. Supernatants were harvested, and IL8 (Cisbio), IL6 (Cisbio), and MCP1 (Mesoscale Discovery, MSD) levels were quantified using commercially available kits following the manufacturer's instructions. To the remaining cell layers was added Cell Titer Glo for 30 min, and luminescence was quantified using a PerkinElmer Microbeta instrument.

RNA Extraction and Library Construction. Total RNA was isolated by using an RNeasy Plant Mini Kit (Qiagen) according to the manufacturer's instructions. Next, the preparation of the mRNA library from total RNA was conducted following the manufacturer's protocol for the Kapa-mRNA-HyperPrep Kit (Roche). Briefly, 750 ng of total RNA was purified by using poly-T oligos attached to magnetic beads and then fragmented by divalent cations at an elevated

temperature. The fragmented RNA undergoes first-strand synthesis using reverse transcriptase and random primers. Second-strand synthesis creates the cDNA fragments using DNA polymerase I and RNaseH. The cDNA fragments then go through end repair, adenylation of the 3′ ends, and ligation of adapters. The cDNA library is enriched using 12 cycles of PCR and purified. Final libraries were assessed using the Agilent Bioanalyzer and Qubit assay methods and then sequenced on an Illumina NextSeq sequencer using a 2 × 75 bp read length.

Quantification of Gene Expression Levels, DEG Analysis, and KEGG Enrichment Analysis. Gene level quantification was performed by first aligning reads against the human reference (GRC38) genome using STAR, followed by running Featurecount with Ensembl version 93. Differential expression analysis was performed using the Limma Bioconductor package. The resulting P values were adjusted using the Benjamini and Hochberg approach for controlling the false discovery rate. Genes with an adjusted P value of <0.05 (FDR < 0.05) determined by Limma and with a fold change value of ≥0.7 between two groups were considered to be differentially expressed.

The Database for Annotation, Visualization and Integrated Discovery (DAVID) was used for systematic and integrative analysis of large gene lists (https://david.ncifcrf.gov/). In our work, the significant GO biological process terms and Kyoto Encyclopedia and Genes and Genomes (KEGG) pathway enrichment analyses of the identified DEGs were performed using DAVID with a $P < 0.001$ threshold.[51,52]

Secreted Cytokine Factor Panel (Human Magnetic Luminex Assay). For small molecule experiments, NHEKs were plated in 96-well plates (10000 cells per well) and incubated overnight. The medium was replaced with hydrocortisone-free Epilife Medium with the HKGS Kit and then treated with escalating doses of JQ1, IBET151, or TPCA1. After a 30 min preincubation, cells were stimulated with 20 ng mL^{-1} TNF and 50 ng mL^{-1} IL17A. Supernatants were harvested 48 h after treatment, frozen, and kept at −80 °C until the assay was run.

For CRISPR/Cas9 knockout experiments, we packaged lentiviral particles containing a nontargeting control ($n = 2$), gRNAs against BRD2, BDR3, and BDR4 (2 gRNAs per gene; $n = 6$ in total), and infected NHEK cells in 60 mm dishes in two or three biological replicates and selected following the procedure described above. After recovery from infection, the medium was replaced with hydrocortisone-free medium, followed by treatment with 50 ng mL^{-1} IL17A and 10 ng mL^{-1} TNF. Supernatants were harvested 24 h after treatment, frozen, and kept at −80 °C until the Luminex assay was run. Cells were subjected to RNA isolation (Qiagen). The sequences for gRNAs were as follows: BRD2 gRNA-1, CACCCCAGCTGCA-ATACCTACACAGTTT; BRD2 gRNA-2, CACCCTTGTTGTA-AATGTAACAGTGTTT; BRD3 gRNA-1, CACCCATCACTGC-AAACGTCACGTGTTT; BRD3 gRNA-2, CACCTGAAGGTAC-ACAGCAAGTGGGTTT; BRD4 gRNA-1, CACCCACCAAACTCCTGAGCATCAGTTT; BRD4 gRNA-2, CACCAGTCGATTTCAATCTCGTCGGTTT; nontargeting control-1 (NTC-1), CACCGACGCCTTGCCCGGCTCACAGTTT; nontargeting control-2 (NTC2), CACCAATCTTACTCGTCCTCC-TTGGTTT.

A custom-designed Human Magnetic Luminex Assay panel from R&D Systems was used to detect and quantify multiple target analytes simultaneously from individual samples. Samples were run exactly according to R&D Systems' Luminex Assay protocol with a 3-fold dilution of the supernatant. The following analytes were examined: CXCL1, CXCL2, CXCL6, CXCL8, GCSF, LCN2, and CCL20. The fluorescent signal associated with individual magnetic beads was read on a Luminex Flexmap 3D. For each sample, the mean fluorescent signal for each analyte was determined. The background signal was subtracted out. Standard curves were generated for each analyte by using Bioplex Manager Software (Bio-Rad Laboratories) using a five-parameter logistic (5-PL) curve fit. Sample quantification of analytes was performed in the Bioplex Manager software relative to standards

for each protein. Two keratinocyte donors were tested with four replicates.

3D Organotypic Raft Experiments. 3D organotypic raft cultures were purchased from MatTek and are supplied with proprietary formulated media. Upon arrival, rafts were equilibrated for 1 day in 5 mL of the medium. On the day of the experiment, the medium was removed and 5 mL of the medium was added for each treatment group. The control represented the medium alone, and treatment groups contained a combination of IL22, IL17A, and TNF (all at 1 ng mL^{-1}) along with 1 μM JQ1, IBET151, or TPCA1. Upon treatment, skin equivalents were placed in the incubator for 3 days. Treatments were replaced on day 2 by removing the treatment and adding fresh treatments. For cytokine release studies, the medium was collected on day 2. For H&E staining, skin equivalents were immediately placed in a 10% neutral buffered formalin solution for 36 h. For qPCR, rafts were frozen. Each data point represents four individual rafts.

Cytokine Release Assays of 3D Organotypic Raft Cultures. MSD V-Plex cytokine kits for human IL6, MCP1, and IL8 were run according to the manufacturer's instructions. Briefly, 25 μL of diluted sample was added to each well and incubated at room temperature for 2 h. After the samples had been removed, three washes were performed with 150 μL of 0.05% (v/v) Tween 20 (Acros) in PBS. Next, 25 μL of a detection antibody solution was then added to each well and incubated for 2 h at room temperature. After removal of the detection antibodies, three washes were performed with 150 μL of 0.05% (v/v) Tween 20 in PBS. The wash buffer was removed; 150 μL of the read buffer was added to each well, and the plate was read using MESO QuickPlex SQ 120. Data represent four individual rafts.

qPCR of 3D Organotypic Raft Cultures. RNA samples were prepared per the manufacturer's instructions in the miRNeasy Mini Kit from Qiagen. For qPCR determination, a CFX384 Real-Time System C1000 Touch Thermocycler was used. Briefly, in a 384-well plate, 2 μL of sample RNA (10 ng μL^{-1}) was added to each well. Eight microliters of TaqMan mix (with appropriate primers) was added to each well. Each measured transcript was presented as a fold change compared to control using the $\Delta\Delta C_T$ method as the RNA fold increase where RPLP0 was used as a housekeeping gene. Data represent four individual rafts.

Histology, IHC, and Imaging of 3D Organotypic Raft Cultures. Formalin-fixed MatTek rafts were placed between two foam biopsy pads in a tissue cassette for FFPE tissue processing (Leica). Postprocessing, a razor blade was used to split the rafts to create two 3 mm wide rectangular samples for embedding. Four-micrometer microtome sections were collected on slides for H&E staining and IHC. All routine H&E staining and IHC were conducted using an autostainer (Leica ST5010) or automated immunostainer (Leica Bond RX). Standardized IHC protocols were used for anti-Ki67 (Ventana), anti-pan cytokeratin (Novus Biologicals), anti-filaggrin, and anti-involucrin staining. All stained tissue slides were digitized for image analysis using a whole slide digital pathology slide scanner with a 20× objective and extended focus scanning parameters (PerkinElmer P250). For quantitative analysis, three raft samples were analyzed per condition for each stain using whole slide digital analysis software (Indica Laboratories HALO). Staining was normalized to the length of the raft sample analyzed.

■ ASSOCIATED CONTENT

Ⓢ Supporting Information

The Supporting Information is available free of charge on the ACS Publications website at DOI: 10.1021/acschem-bio.8b00260.

Effects of IL17A and TNF, including quality control metrics for screening on six unique keratinocyte donors (Supplementary Table 1), genes identified from RNA-Seq analysis with less sensitivity (Supplementary Table 2) or increased sensitivity (Supplementary Table 3) to IL17A and TNF, KEGG pathway enrichment analysis of RNA-Seq data (Supplementary Table 4), comparison of

IL8 staining and secretion in keratinocytes after treatment with the TNNI3K inhibitor (Supplementary Figure 1), inhibition of responses primary keratinocytes and HS27 fibroblasts to IL17A/TNF with IBET151 (Supplementary Figure 2), BRD2 knockout HS27 dermal fibroblasts that are resistant to IL17A/TNF stimulation (Supplementary Figure 3), individual performance among BRD2, BRD3, and BRD4 gRNAs in pooled CRISPR screening (Supplementary Figure 4), effects of BRD2 or IKKαβ inhibition on 3D organotypic skin raft architecture in the absence of IL17A, TNF, and IL22 (Supplementary Figure 5), overview of screening libraries and target hypotheses identified through screening (Supplementary Figure 6), barcode distribution in IL8 low, IL8 high, and IL8 remaining keratinocytes after CRISPR screening (Supplementary Figure 7), and rates of recovery of the CRISPR library in IL8 low, IL8 high, and IL8 remaining keratinocytes (Supplementary Figure 8) (PDF)

■ AUTHOR INFORMATION

Corresponding Author
*AbbVie Bioresearch Center, 100 Research Dr., Worcester, MA 01605. E-mail: peter.slivka@abbvie.com.

ORCID ⓘ
Peter F. Slivka: 0000-0003-2047-3668

Author Contributions
∇P.F.S. and C.-L.H. contributed equally to this work.

Notes
The authors declare the following competing financial interest(s): The design, study conduct, and financial support for this research were provided by AbbVie. AbbVie participated in the interpretation of data and review and approval of the publication.

■ REFERENCES

(1) Jin, W., and Dong, C. (2013) IL-17 cytokines in immunity and inflammation. *Emerging Microbes Infect.* 2, No. e60.

(2) Murugaiyan, G., and Saha, B. (2009) Protumor vs antitumor functions of IL-17. *J. Immunol.* 183, 4169–4175.

(3) Gaffen, S. L., Jain, R., Garg, A. V., and Cua, D. J. (2014) The IL-23-IL-17 immune axis: from mechanisms to therapeutic testing. *Nat. Rev. Immunol.* 14, 585–600.

(4) Wasilewska, A., Winiarska, M., Olszewska, M., and Rudnicka, L. (2016) Interleukin-17 inhibitors. A new era in treatment of psoriasis and other skin diseases. *Postepy Dermatol Alergol* 4, 247–252.

(5) Rizvi, S., Chaudhari, K., and Syed, B. A. (2015) The psoriasis drugs market. *Nat. Rev. Drug Discovery* 14, 745–746.

(6) Raychaudhuri, S. P. (2013) Role of IL-17 in psoriasis and psoriatic arthritis. *Clin. Rev. Allergy Immunol.* 44, 183–193.

(7) Amatya, N., Garg, A. V., and Gaffen, S. L. (2017) IL-17 Signaling: The Yin and the Yang. *Trends Immunol.* 38, 310–322.

(8) Wu, L., Chen, X., Zhao, J., Martin, B., Zepp, J. A., Ko, J. S., Gu, C., Cai, G., Ouyang, W., Sen, G., Stark, G. R., Su, B., Vines, C. M., Tournier, C., Hamilton, T. A., Vidimos, A., Gastman, B., Liu, C., and Li, X. (2015) A novel IL-17 signaling pathway controlling keratinocyte proliferation and tumorigenesis via the TRAF4-ERK5 axis. *J. Exp. Med.* 212, 1571–1587.

(9) Rabeony, H., Petit-Paris, I., Garnier, J., Barrault, C., Pedretti, N., Guilloteau, K., Jegou, J. F., Guillet, G., Huguier, V., Lecron, J. C., Bernard, F. X., and Morel, F. (2014) Inhibition of keratinocyte differentiation by the synergistic effect of IL-17A, IL-22, IL-1alpha, TNFalpha and oncostatin M. *PLoS One* 9, No. e101937.

(10) Martin, D. A., Towne, J. E., Kricorian, G., Klekotka, P., Gudjonsson, J. E., Krueger, J. G., and Russell, C. B. (2013) The emerging role of IL-17 in the pathogenesis of psoriasis: preclinical and clinical findings. *J. Invest. Dermatol.* 133, 17–26.

(11) Huh, J. R., and Littman, D. R. (2012) Small molecule inhibitors of RORgammat: targeting Th17 cells and other applications. *Eur. J. Immunol.* 42, 2232–2237.

(12) Mele, D. A., Salmeron, A., Ghosh, S., Huang, H. R., Bryant, B. M., and Lora, J. M. (2013) BET bromodomain inhibition suppresses TH17-mediated pathology. *J. Exp. Med.* 210, 2181–2190.

(13) Liu, S., Dakin, L. A., Xing, L., Withka, J. M., Sahasrabudhe, P. V., Li, W., Banker, M. E., Balbo, P., Shanker, S., Chrunyk, B. A., Guo, Z., Chen, J. M., Young, J. A., Bai, G., Starr, J. T., Wright, S. W., Bussenius, J., Tan, S., Gopalsamy, A., Lefker, B. A., Vincent, F., Jones, L. H., Xu, H., Hoth, L. R., Geoghegan, K. F., Qiu, X., Bunnage, M. E., and Thorarensen, A. (2016) Binding site elucidation and structure guided design of macrocyclic IL-17A antagonists. *Sci. Rep.* 6, 30859.

(14) Ha, H. L., Wang, H., Pisitkun, P., Kim, J. C., Tassi, I., Tang, W., Morasso, M. I., Udey, M. C., and Siebenlist, U. (2014) IL-17 drives psoriatic inflammation via distinct, target cell-specific mechanisms. *Proc. Natl. Acad. Sci. U. S. A.* 111, E3422–3431.

(15) El Malki, K., Karbach, S. H., Huppert, J., Zayoud, M., Reissig, S., Schuler, R., Nikolaev, A., Karram, K., Munzel, T., Kuhlmann, C. R., Luhmann, H. J., von Stebut, E., Wortge, S., Kurschus, F. C., and Waisman, A. (2013) An alternative pathway of imiquimod-induced psoriasis-like skin inflammation in the absence of interleukin-17 receptor a signaling. *J. Invest. Dermatol.* 133, 441–451.

(16) Skvara, H., Dawid, M., Kleyn, E., Wolff, B., Meingassner, J. G., Knight, H., Dumortier, T., Kopp, T., Fallahi, N., Stary, G., Burkhart, C., Grenet, O., Wagner, J., Hijazi, Y., Morris, R. E., McGeown, C., Rordorf, C., Griffiths, C. E., Stingl, G., and Jung, T. (2008) The PKC inhibitor AEB071 may be a therapeutic option for psoriasis. *J. Clin. Invest.* 118, 3151–3159.

(17) Roller, A., Perino, A., Dapavo, P., Soro, E., Okkenhaug, K., Hirsch, E., and Ji, H. (2012) Blockade of phosphatidylinositol 3-kinase PI3Kdelta or PI3Kgamma reduces IL-17 and ameliorates imiquimod-induced psoriasis-like dermatitis. *J. Immunol.* 189, 4612–4620.

(18) Welsh, S. J., and Corrie, P. G. (2015) Management of BRAF and MEK inhibitor toxicities in patients with metastatic melanoma. *Ther. Adv. Med. Oncol.* 7, 122–136.

(19) Cheung, K., Lu, G., Sharma, R., Vincek, A., Zhang, R., Plotnikov, A. N., Zhang, F., Zhang, Q., Ju, Y., Hu, Y., Zhao, L., Han, X., Meslamani, J., Xu, F., Jaganathan, A., Shen, T., Zhu, H., Rusinova, E., Zeng, L., Zhou, J., Yang, J., Peng, L., Ohlmeyer, M., Walsh, M. J., Zhang, D. Y., Xiong, H., and Zhou, M. M. (2017) BET N-terminal bromodomain inhibition selectively blocks Th17 cell differentiation and ameliorates colitis in mice. *Proc. Natl. Acad. Sci. U. S. A.* 114, 2952–2957.

(20) Filippakopoulos, P., Qi, J., Picaud, S., Shen, Y., Smith, W. B., Fedorov, O., Morse, E. M., Keates, T., Hickman, T. T., Felletar, I., Philpott, M., Munro, S., McKeown, M. R., Wang, Y., Christie, A. L., West, N., Cameron, M. J., Schwartz, B., Heightman, T. D., La Thangue, N., French, C. A., Wiest, O., Kung, A. L., Knapp, S., and Bradner, J. E. (2010) Selective inhibition of BET bromodomains. *Nature* 468, 1067–1073.

(21) Dawson, M. A., Prinjha, R. K., Dittmann, A., Giotopoulos, G., Bantscheff, M., Chan, W. I., Robson, S. C., Chung, C. W., Hopf, C., Savitski, M. M., Huthmacher, C., Gudgin, E., Lugo, D., Beinke, S., Chapman, T. D., Roberts, E. J., Soden, P. E., Auger, K. R., Mirguet, O., Doehner, K., Delwel, R., Burnett, A. K., Jeffrey, P., Drewes, G., Lee, K., Huntly, B. J., and Kouzarides, T. (2011) Inhibition of BET recruitment to chromatin as an effective treatment for MLL-fusion leukaemia. *Nature 478*, 529−533.

(22) Eskandarpour, M., Alexander, R., Adamson, P., and Calder, V. L. (2017) Pharmacological Inhibition of Bromodomain Proteins Suppresses Retinal Inflammatory Disease and Downregulates Retinal Th17 Cells. *J. Immunol. 198*, 1093−1103.

(23) Taniguchi, Y. (2016) The Bromodomain and Extra-Terminal Domain (BET) Family: Functional Anatomy of BET Paralogous Proteins. *Int. J. Mol. Sci. 17*, 1849.

(24) Klein, K., Kabala, P. A., Grabiec, A. M., Gay, R. E., Kolling, C., Lin, L. L., Gay, S., Tak, P. P., Prinjha, R. K., Ospelt, C., and Reedquist, K. A. (2016) The bromodomain protein inhibitor I-BET151 suppresses expression of inflammatory genes and matrix degrading enzymes in rheumatoid arthritis synovial fibroblasts. *Ann. Rheum. Dis. 75*, 422−429.

(25) Muller, S., Filippakopoulos, P., and Knapp, S. (2011) Bromodomains as therapeutic targets. *Expert Rev. Mol. Med. 13*, No. e29.

(26) Trousdale, R. K., and Wolgemuth, D. J. (2004) Bromodomain containing 2 (Brd2) is expressed in distinct patterns during ovarian folliculogenesis independent of FSH or GDF9 action. *Mol. Reprod. Dev. 68*, 261−268.

(27) Tsume, M., Kimura-Yoshida, C., Mochida, K., Shibukawa, Y., Amazaki, S., Wada, Y., Hiramatsu, R., Shimokawa, K., and Matsuo, I. (2012) Brd2 is required for cell cycle exit and neuronal differentiation through the E2F1 pathway in mouse neuroepithelial cells. *Biochem. Biophys. Res. Commun. 425*, 762−768.

(28) Eckhart, L., Lippens, S., Tschachler, E., and Declercq, W. (2013) Cell death by cornification. *Biochim. Biophys. Acta, Mol. Cell Res. 1833*, 3471−3480.

(29) Fischer, H., Langbein, L., Reichelt, J., Praetzel-Wunder, S., Buchberger, M., Ghannadan, M., Tschachler, E., and Eckhart, L. (2014) Loss of keratin K2 expression causes aberrant aggregation of K10, hyperkeratosis, and inflammation. *J. Invest. Dermatol. 134*, 2579−2588.

(30) Sasamoto, Y., Hayashi, R., Park, S. J., Saito-Adachi, M., Suzuki, Y., Kawasaki, S., Quantock, A. J., Nakai, K., Tsujikawa, M., and Nishida, K. (2016) PAX6 Isoforms, along with Reprogramming Factors, Differentially Regulate the Induction of Cornea-specific Genes. *Sci. Rep. 6*, 20807.

(31) Hwang, S. Y., Kim, J. Y., Kim, K. W., Park, M. K., Moon, Y., Kim, W. U., and Kim, H. Y. (2004) IL-17 induces production of IL-6 and IL-8 in rheumatoid arthritis synovial fibroblasts via NF-kappaB- and PI3-kinase/Akt-dependent pathways. *Arthritis Res. Ther. 6*, R120−128.

(32) Laan, M., Lotvall, J., Chung, K. F., and Linden, A. (2001) IL-17-induced cytokine release in human bronchial epithelial cells in vitro: role of mitogen-activated protein (MAP) kinases. *Br. J. Pharmacol. 133*, 200−206.

(33) Chiricozzi, A., Guttman-Yassky, E., Suarez-Farinas, M., Nograles, K. E., Tian, S., Cardinale, I., Chimenti, S., and Krueger, J. G. (2011) Integrative responses to IL-17 and TNF-alpha in human keratinocytes account for key inflammatory pathogenic circuits in psoriasis. *J. Invest. Dermatol. 131*, 677−687.

(34) Gabr, M. A., Jing, L., Helbling, A. R., Sinclair, S. M., Allen, K. D., Shamji, M. F., Richardson, W. J., Fitch, R. D., Setton, L. A., and Chen, J. (2011) Interleukin-17 synergizes with IFNgamma or TNFalpha to promote inflammatory mediator release and intercellular adhesion molecule-1 (ICAM-1) expression in human intervertebral disc cells. *J. Orthop. Res. 29*, 1−7.

(35) Chabaud, M., Fossiez, F., Taupin, J. L., and Miossec, P. (1998) Enhancing effect of IL-17 on IL-1-induced IL-6 and leukemia inhibitory factor production by rheumatoid arthritis synoviocytes and its regulation by Th2 cytokines. *J. Immunol. 161*, 409−414.

(36) Wilson, V. G. (2013) Growth and differentiation of HaCaT keratinocytes. *Methods Mol. Biol. 1195*, 33−41.

(37) Chaturvedi, V., Qin, J. Z., Denning, M. F., Choubey, D., Diaz, M. O., and Nickoloff, B. J. (1999) Apoptosis in proliferating, senescent, and immortalized keratinocytes. *J. Biol. Chem. 274*, 23358−23367.

(38) Baek, J. H., Lee, G., Kim, S. N., Kim, J. M., Kim, M., Chung, S. C., and Min, B. M. (2003) Common genes responsible for differentiation and senescence of human mucosal and epidermal keratinocytes. *Int. J. Mol. Med. 12*, 319−325.

(39) Walko, G., Woodhouse, S., Pisco, A. O., Rognoni, E., Liakath-Ali, K., Lichtenberger, B. M., Mishra, A., Telerman, S. B., Viswanathan, P., Logtenberg, M., Renz, L. M., Donati, G., Quist, S. R., and Watt, F. M. (2017) A genome-wide screen identifies YAP/WBP2 interplay conferring growth advantage on human epidermal stem cells. *Nat. Commun. 8*, 14744.

(40) Belkina, A. C., Nikolajczyk, B. S., and Denis, G. V. (2013) BET protein function is required for inflammation: Brd2 genetic disruption and BET inhibitor JQ1 impair mouse macrophage inflammatory responses. *J. Immunol. 190*, 3670−3678.

(41) Cheung, K. L., Zhang, F., Jaganathan, A., Sharma, R., Zhang, Q., Konuma, T., Shen, T., Lee, J. Y., Ren, C., Chen, C. H., Lu, G., Olson, M. R., Zhang, W., Kaplan, M. H., Littman, D. R., Walsh, M. J., Xiong, H., Zeng, L., and Zhou, M. M. (2017) Distinct Roles of Brd2 and Brd4 in Potentiating the Transcriptional Program for Th17 Cell Differentiation. *Mol. Cell 65*, 1068−1080.

(42) Gordon, K., Kochkodan, J. J., Blatt, H., Lin, S. Y., Kaplan, N., Johnston, A., Swindell, W. R., Hoover, P., Schlosser, B. J., Elder, J. T., Gudjonsson, J. E., and Getsios, S. (2013) Alteration of the EphA2/Ephrin-A signaling axis in psoriatic epidermis. *J. Invest. Dermatol. 133*, 712−722.

(43) Liu, Y., Zhu, H., Su, Z., Sun, C., Yin, J., Yuan, H., Sandoghchian, S., Jiao, Z., Wang, S., and Xu, H. (2012) IL-17 contributes to cardiac fibrosis following experimental autoimmune myocarditis by a PKCbeta/Erk1/2/NF-kappaB-dependent signaling pathway. *Int. Immunol. 24*, 605−612.

(44) Baud, M. G. J., Lin-Shiao, E., Cardote, T., Tallant, C., Pschibul, A., Chan, K. H., Zengerle, M., Garcia, J. R., Kwan, T. T., Ferguson, F. M., and Ciulli, A. (2014) Chemical biology. A bump-and-hole approach to engineer controlled selectivity of BET bromodomain chemical probes. *Science 346*, 638−641.

(45) Zhang, G., Sanchez, R., and Zhou, M. M. (2012) Scaling the druggability landscape of human bromodomains, a new class of drug targets. *J. Med. Chem. 55*, 7342−7345.

(46) Nestle, F. O., Di Meglio, P., Qin, J. Z., and Nickoloff, B. J. (2009) Skin immune sentinels in health and disease. *Nat. Rev. Immunol. 9*, 679−691.

(47) Wang, F., Liu, H., Blanton, W. P., Belkina, A., Lebrasseur, N. K., and Denis, G. V. (2010) Brd2 disruption in mice causes severe obesity without Type 2 diabetes. *Biochem. J. 425*, 71−83.

(48) Chin, S. S., Romano, R. A., Nagarajan, P., Sinha, S., and Garrett-Sinha, L. A. (2013) Aberrant epidermal differentiation and disrupted DeltaNp63/Notch regulatory axis in Ets1 transgenic mice. *Biol. Open 2*, 1336−1345.

(49) Candi, E., Schmidt, R., and Melino, G. (2005) The cornified envelope: a model of cell death in the skin. *Nat. Rev. Mol. Cell Biol. 6*, 328−340.

(50) Li, W., Xu, H., Xiao, T., Cong, L., Love, M. I., Zhang, F., Irizarry, R. A., Liu, J. S., Brown, M., and Liu, X. S. (2014) MAGeCK enables robust identification of essential genes from genome-scale CRISPR/Cas9 knockout screens. *Genome Biol. 15*, 554.

(51) Kanehisa, M., Sato, Y., Kawashima, M., Furumichi, M., and Tanabe, M. (2016) KEGG as a reference resource for gene and protein annotation. *Nucleic Acids Res. 44*, D457−462.

(52) Kanehisa, M., and Goto, S. (2000) KEGG: kyoto encyclopedia of genes and genomes. *Nucleic Acids Res. 28*, 27−30.